



NATIONAL ENERGY TECHNOLOGY LABORATORY



Natural Gas Hydrates Research Portfolio

Quarterly Progress Report

FY15-Q3

Yongkoo Seol, Technical Portfolio Lead

Delivery Date: July 30, 2015

Prepared by
U.S. Department of Energy
National Energy Technology Laboratory
Office of Research and Development

Prepared for
U.S. Department of Energy
National Energy Technology Laboratory
Strategic Center for Natural Gas and Oil



List of Authors

Yongkoo Seol, ORD Technical Portfolio Lead

Gary Sames, ORD Project Coordinator

Cynthia Powell, ORD Focus Area Lead (*Acting*)

Jeffery Ilconich, Activity Manager

Table of Contents

1.0 Annual Executive Summary	1
2.0 Milestones	1
3.0 FY Budgetary Information	4
4.0 Technical Progress	5
Fiscal Year 2015 Quarter 1	5
Accomplishments.....	5
Forecast for Next 6 Months	14
Products	16
Changes/Problems	16
Fiscal Year 2015 Quarter 2	17
Accomplishments.....	17
Forecast for Next 6 Months	46
Products	48
Changes/Problems	48
Fiscal Year 2015 Quarter 3	49
Accomplishments.....	49
Forecast for Next 6 Months	62
Products	64
Changes/Problems	64
Appendix A: Participating and Other Collaborating Organizations	A-1

Acronym List

Acronym	Descriptive Name
2D	Two-Dimensional
3D	Three-Dimensional
AGH	Aqueous-Gas-Hydrate
AK-DNR	Alaskan Department of Natural Resources
ANS	Alaska North Slope
Be	Beryllium
CMU	Carnegie Mellon University
CO ₂	Carbon Dioxide
CSM	Colorado School of Mines
CT	Computed Tomography
DOE	Department of Energy
DT	Sonic
FAL	Focus Area Lead
FEHM	Finite Element/Finite Volume Heat and Mass Transfer Computer Code
FWP	Field Work Proposal
GR	Gamma Ray
GUI	Graphical User Interface
HBS	Hydrate-Bearing Sediment
HQ	Headquarters
HRS	HydrateResSim
HSZ	Hydrate Stability Zone
MST	Multi-Stage Tests
NETL	National Energy Technology Laboratory
NMR	Nuclear Magnetic Resonance
ORD	Office of Research and Development
PBU	Prudhoe Bay Unit
PID	Proportional-Integral-Derivative
Pitt	University of Pittsburgh
PMO	Project Management Office
PMP	Project Management Plan
PSIG	Pounds per Square Inch Gauge
PSU or Penn State	The Pennsylvania State University
R&D	Research and Development
Res	Resistivity
RES	Research and Engineering Services

Acronym	Descriptive Name
SARS	Safety Analysis and Review System
SCNGO	Strategic Center for Natural Gas and Oil
S _H	Hydrate Saturation
SHC	Shale Content
SMP	Spatially Mobilized Plane
SOPO	Statement of Project Objectives
SSR	Solid-State Relay
SST	Single-Stage Tests
S _w	Water Saturation
TCD	Thermal Conductivity Detector
THF	Tetrahydrofuran
THM	Thermal-Hydrological-Geomechanical
TM	Technology Manager
TMo	Technical Monitor
TPL	Technical Portfolio Lead
TTP	Thermal Transfer Plate
TVDSS	Total Vertical Depth
USGS	United States Geological Survey
V _{sh}	Shale Volume
VSHC	Volume of Shale Content
WVU	West Virginia University

1.0 Annual Executive Summary

The Annual Executive Summary will be provided in the FY15-Q4 Report.

2.0 Milestones

The status of the M-1 milestones is presented below in Table 1.

Table 1: Major Goals of the Project

Milestone Identifier	Milestone Title	Planned Completion Date	Actual/ Forecast Completion	Method of Verification	Comments
Outstanding FY14 Milestones					
M1.14.3.B	Complete data analysis for tri-axial tests and development of a constitutive model defining the relationship between hydrate saturation and elastoplastic soil behavior parameters.	09/30/2014	11/14/2014	Manuscripts on the testing program and constitutive modeling (Subtask 3.2, 09/14).	Complete
Task 2.0 Reservoir Simulation of Gas Hydrates Production Field Tests					
M1.15.2.A	Analysis of Iġnik Sikumi #1 code comparison problem for code comparison and analysis.	03/31/2015	03/31/2015	Series of manuscripts on the Iġnik Sikumi history match from the Code Comparison Group (Subtask 2.2).	Complete. No code comparison partners identified. Task complete.
M1.15.2.B	Complete simulations of production and flow modeling from a long-term depressurization test at the site chosen for the field test.	06/30/2015	06/30/2015	Manuscript on depressurization test scenarios on the Alaska North Slope (Subtask 2.1).	Complete
M1.15.2.C	Analysis of a Marine hydrate-based problem for code comparison and analysis.	09/30/2015	09/30/2015	Problem sets developed and shared with collaboration partners (Subtask 2.2).	On Schedule

Milestone Identifier	Milestone Title	Planned Completion Date	Actual/Forecast Completion	Method of Verification	Comments
Task 3.0 Laboratory Hydrologic and Geomechanical Characterization and Analysis of Hydrate-Bearing Sediments					
M1.15.3.A	Demonstration of core flow equipment and personnel capability to conduct the relative permeability test on hydrate-bearing sediments.	03/31/2015	08/31/2015	Improved mobile gas hydrate testing unit with additional gas/fluid mass flow meters and temperature chamber (Subtask 3.1).	Delayed. Staffing for the task is delayed. Equipment (fluid separator, back-pressure regulator, etc.) is to be delivered by mid-April. New Actual/Forecast Completion date is 8/31/2015, 2015.ORD-TPL notified SCNGO of delay on 6/5/2015 via email.
M1.15.3.B	Complete relative permeability tests on various types of sediment textures at different hydrate saturations and effective confining stresses and porosities.	03/30/2015	09/30/2015	Report on relative permeability of HBS (Subtask 3.1).	Delayed. Staffing for the task is delayed. Equipment (fluid separator, back-pressure regulator, etc.) is to be delivered by mid-August. New Actual/Forecast Completion of 9/30/2015. TPL notified SCNGO of delay on 6/15/2015.
M1.15.3.C	Complete a working TOUGH+FLAC framework.	06/30/2015	08/28/2015	A working TOUGH+FLAC code incorporated constitutive laws for hydrate-bearing soils (Subtask 3.3).	Staff has been just identified and initiated the task on 6/1/15. ORD-TPL notified SCNGO of delay on 6/5/15 via email.
M1.15.3.D	Complete tri-axial geomechanical strength and deformability tests on dissociated HBS at various dissociation levels.	06/30/2015	09/30/2015	Manuscript on geomechanical strength tests on hydrate-bearing sediment under dissociation condition (Subtask 3.2).	Staff has been just identified and initiated the task on 6/1/15. ORD-TPL notified SCNGO of delay on 6/5/15 via email.

Milestone Identifier	Milestone Title	Planned Completion Date	Actual/ Forecast Completion	Method of Verification	Comments
M1.15.3.E	Complete data analysis for tri-axial tests and development of a constitutive model.	09/30/2015	09/30/2015	Manuscripts on the geomechanical tests for HBS under hydrate dissociation condition and constitutive modeling (Subtask 3.3).	Staff has been just identified and initiated the task on 6/1/15. ORD-TPL notified SCNGO of delay on 6/5/15 via email.
Task 4.0 Pore-Scale Visualization and Characterization of Hydrate-Bearing Sediments					
M1.15.4.A	Complete visualization of hydrate evolutions during brine injection and validate the NETL proposed non-cementing hydrate formation method.	03/31/2015	03/31/2015	Report on hydrate evolutions during continuous saline flow and images/videos on this dynamic process (Subtask 4.1).	Complete. Hydrate visualization with high resolution micro CT completed.
M1.15.4.B	Complete design, modification, and manufacture of end pieces for current high-pressure X-ray microCT vessel to have geomechanical measurement capabilities.	06/30/2015	06/30/2015	Manuscript on understanding permeability in sediments under heterogeneous pressure distribution during hydrate dissociation (Subtask 4.2).	Complete
M1.15.4.C	Complete X-ray micro CT imaging for water and gas distributions after hydrate dissociation and implication of flow permeability during dissociation.	09/30/2015	09/30/2015	Report on process monitoring using wave velocity and CT scanning in hydrate-bearing sediments, focusing on effects of hydrate morphology, particularly for common hydrate morphologies in nature such as patchy and veins (Subtask 4.3).	On Schedule
M1.15.4.D	Development of a microfluidic, 2D system for flow and permeability determination.	09/30/2015	09/30/2015	Report on the 2D Microfluidic flow tests (Subtask 4.4).	On Schedule

Note: Gray highlighting from the Hydrates FY15 FWP and FY15 PMP was removed from this quarterly progress report since funding was received and qualified researchers or students were identified for full staff support.

3.0 FY Budgetary Information

The variance from the FY14 funding for the Natural Gas Hydrates program is funding and supporting the RES contract effort through the end of the current RES contract. No FY15 funding currently supports efforts related to the site support contract.

The cost performance histogram is provided below (Figure 1) to show the planned and actual cost performance for the Natural Gas Hydrates Research Portfolio.

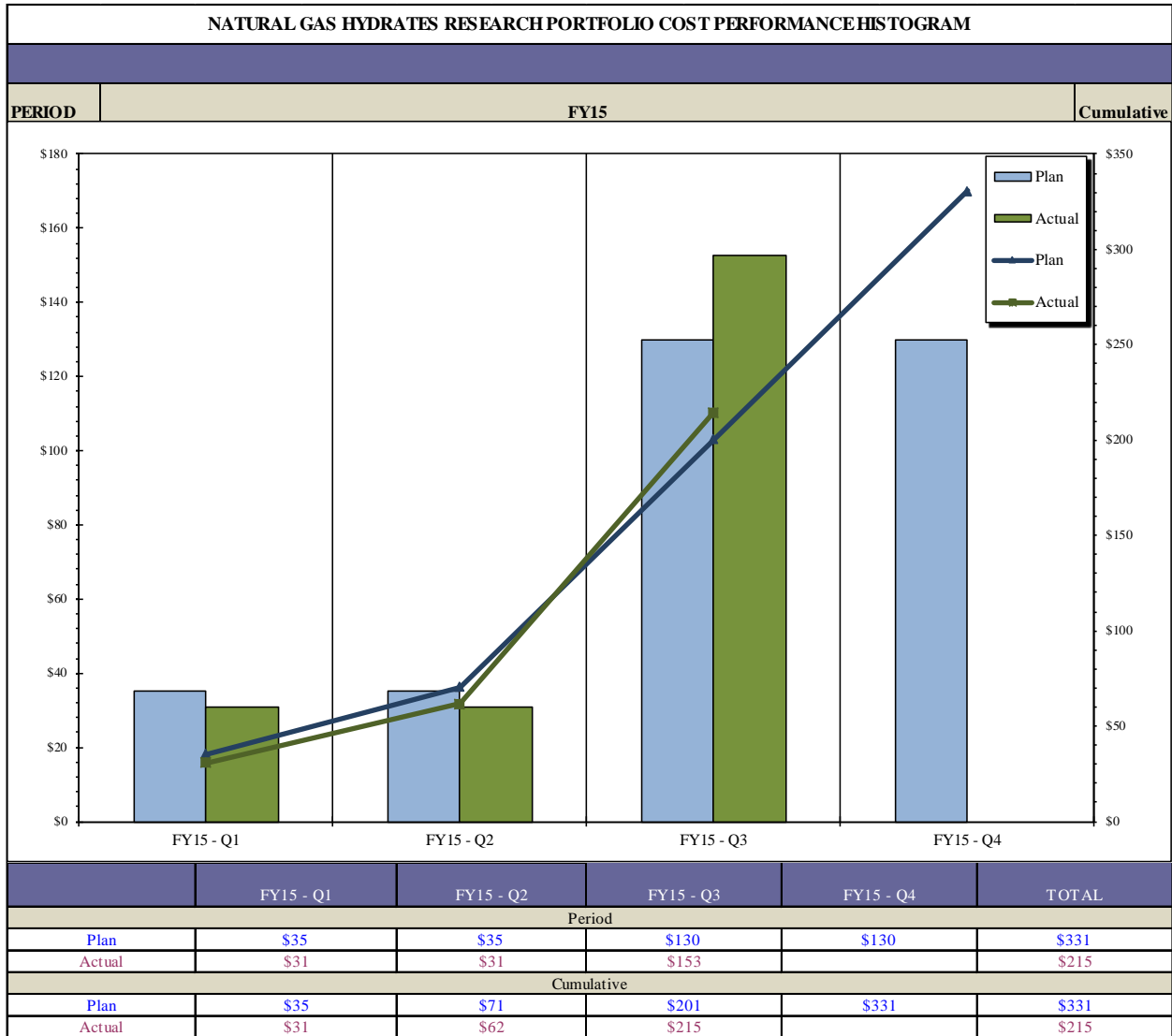


Figure 1: FY15 Natural Gas Hydrates Research Portfolio cost performance histogram (\$ x 1,000).

Variance Explanation

The budget (plan) for the FY15 third quarter was \$130K while the actual cost was \$153K, resulting in a cost variance of -\$23K. Cumulative to date, the budget (plan) was \$200K while the actual cost was \$215K, resulting in a cost variance of -\$15K. Carryover from prior fiscal years was planned for and is making up for the shortfall in FY15 funding.

4.0 Technical Progress

Fiscal Year 2015 Quarter 1

Accomplishments

Task 1.0 Project Management and Outreach

All project management deliverables from the NETL Office of Research and Development (ORD) to the Strategic Center for Natural Gas and Oil (SCNGO) were delivered on time with support from the Project Management Office (PMO). Deliverables inclusive of reports to SCNGO, task and subtask meetings, monthly invoice reviews with URS/AECOM, and milestone tracking were all met within the scheduled timeframe. SCNGO can access their required deliverables via SharePoint at: <http://prod65-share4.netl.doe.gov/sites/ORD-PMO/Pages/SCNGO.aspx>.

The FY15-Q1 deliverables included:

- The FY14-Q4 Report was submitted to SCNGO on November 20, 2014.
- As per new SCNGO guidance, the progress reports for Q1, Q2, Q3, and Q4 were cumulated with an annual executive summary to serve as the annual report deliverable.

Technical writing, deliverable coordination, and project controls support were provided by the PMO.

Task 2.0 Reservoir Simulation of Gas Hydrates Production Field Tests

Subtask 2.1 Alaska North Slope Production Test Simulation Assistance

- A 3D heterogeneous Site 2 model was constructed. Site 2 is a theoretically deeper Mt. Elbert-like deposit which might be encountered within the Milne point unit. Since the reservoir depth of Site 2 is yet unknown, a series of simulations were run with a range of reservoir depths varying from 570 – 670 m. Gas rate profiles show that higher gas rates are obtained with an increase in reservoir depth. These results are reasonable because the relatively higher temperatures of deeper reservoirs increase instability of the hydrates which make them dissociate readily.
- A framework for conducting flow assurance studies in production wellbore was designed. This was done by developing a transient 2D temperature model in a two-phase vertical wellbore water+gas system with hydrate formation using the approach of computational fluid dynamics. An annulus growth of the hydrate propensity field was observed within the wellbore.
- The next steps will involve conducting sensitivity runs and uncertainty analyses on Site 2 with respect to the distribution of hydrate saturation and porosity.

The wellbore models will be refined by relaxing some of the assumptions to improve on their validity and accuracy.

Subtask 2.2 International Code Comparison Continuation – Ignik Sikumi History Match Analysis and Marine Deposit Based on the 2013 Nankai Trough Test or Other Marine Sites

Different numerical simulation scenarios were considered with a focus on understanding the CO₂ injection into the hydrate bearing sands of the permafrost regions. The recent, primary focus is on the formations of the Prudhoe-Bay L-Pad regions.

Summary of work completed in FY14-Q4:

- Numerical simulations were done to study the migration of CO₂ in the hydrate formations of the Prudhoe Bay site. CO₂-Hydrate is more stable than CH₄-Hydrate only at lower pressures (until 285 K); therefore, the top of HSZ (Hydrate Stability Zone) of CH₄ was deeper than the top of HSZ of CO₂. The reservoir domains were considered as two different zones, Zone-1 being CH₄-CO₂ Hydrate (AGH state variable was assigned) and Zone-2 as CH₄-CO₂-Hydrate. In these simulations: (1) gaseous CO₂ was injected near the top of CH₄ HSZ at a particular pressure and temperature conditions and (2) CH₄ production well was modeled as a surface boundary nearly 50 m away from the origin. CH₄ production is achieved by depressurizing the domain. Different numerical simulations were performed by changing the state variables of Zones 1 and 2.
- The accomplishments primarily involved studying the CO₂ flow in an inclined reservoir modeling the reservoir conditions of the Prudhoe Bay L-Pad region. The trend of the pressure, temperature, and CH₄-CO₂-Hydrate compositional changes in the formations due to the injection of CO_{2(g)} and CO_{2(AqG)} at the top of the hydrate stability zone of CH₄ hydrate was studied.

Task 3.0 Laboratory Hydrologic and Geomechanical Characterization and Analysis of Hydrate-Bearing Sediments

Subtask 3.1 Laboratory Measurement of Relative Permeability of CH₄ Gas in Brine-Saturated Hydrate-Bearing Sediments

Relative permeability of CH₄ gas in hydrate-bearing sediments (HBS) is a key parameter for numerical simulations and is yet to be determined with relevant samples. In FY15-Q1, this task focused mainly on the planning and development of a new experimental setup to properly measure the relative permeability based on existing mobile carts.

- A literature review was conducted. Few studies, regarding “gas-water” relative permeability in hydrate-bearing sediments, were found. The lack of studies in this particular issue was most likely due to difficulties in inhibiting hydrate phase change (hydrate formation/dissociation) during gas/water flooding. Most relevant studies were more related to effective permeability measurements of hydrate-bearing sediments during water flooding.
- Preliminary design of test setup was proposed (Figure 2). The validity of the design will be examined in consideration of targeted data collection for gas-water relative permeability measurement in hydrate-bearing sediments. Test equipment and parts, which also includes an electronically-controlled back pressure regulator and a two-phase sonic fluid separator, are to be accordingly obtained.

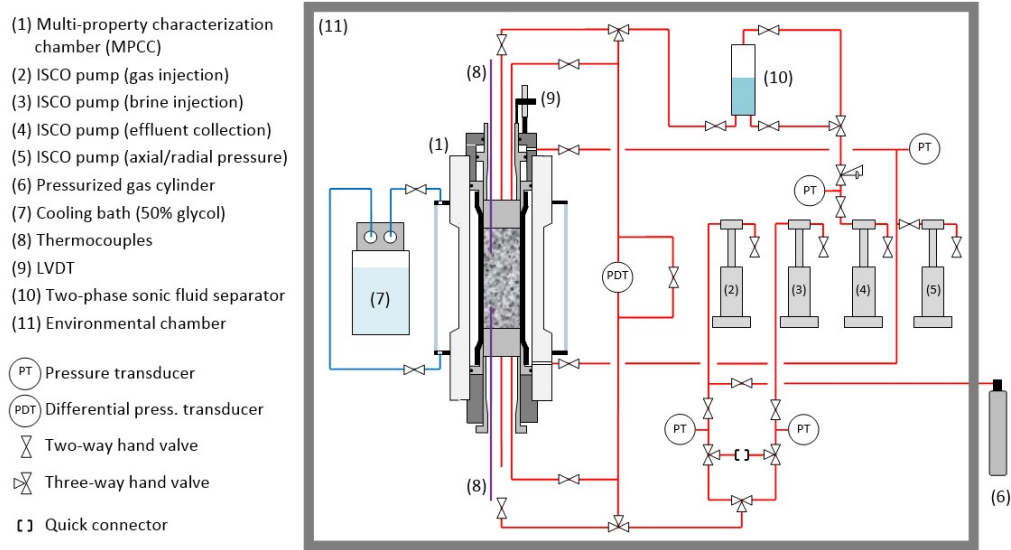


Figure 2: Proposed test setup for relative permeability measurement of hydrate-bearing sediments.

- A plan for upgrading an existing environmental chamber was proposed. The environmental chamber will eventually accommodate our core-flow-test mobile cart (Figure 2), so that the test can be conducted under better control of temperature (less temperature fluctuation).

Subtask 3.2 Tri-Axial Compression Tests on Hydrate-Bearing Sediments with Induced Hydrate Dissociation under Shear Stress

Understanding of geomechanical response of hydrate-bearing sediments (HBS) to hydrate dissociation is critical to safely exploit hydrate accumulations for gas production. In FY15-Q1, a preliminary plan to complete a geomechanical test on HBS subjected to dissociation was proposed to evaluate the deformability of HBS subjected to various scenarios of dissociation.

- A literature review has been conducted to propose an experimental plan for this study.
- Geomechanical tests, based on the proposed preliminary test plan, consist of:
 1. Four core samples
 - Host material: F110 silica sand + 5% Kaolinite Clay
 - Brine-saturated non-cementing HBS sample
 - Initial hydrate saturation, $S_h = \sim 40\%$
 2. Hydrate dissociation method
 - Depressurization (two samples)
 - Thermal recovery (two samples)
 3. Tri-axial drainage compression test during hydrate dissociation
 - Effective confining pressure, $\sigma'_o = 0.69$ MPa
 - Deviator stress, q (effective axial – radial pressure), at which the hydrate dissociation is initiated:

50% (~1.5 MPa) and 130% (~4 MPa) of peak deviator stress, q_{peak} of host sample (~3 MPa)

- q will be applied on the HBS sample up to 50% or 130% of q_{peak} of host sample. Hydrate will then be dissociated by either depressurization or thermal recovery method while maintaining the same axial and radial pressures, at which the dissociation is started. The axial strain, axial, radial, and pore pressures will be continuously measured during the entire course of the experiment to establish the stress-strain relationship, as shown in Figure 3.

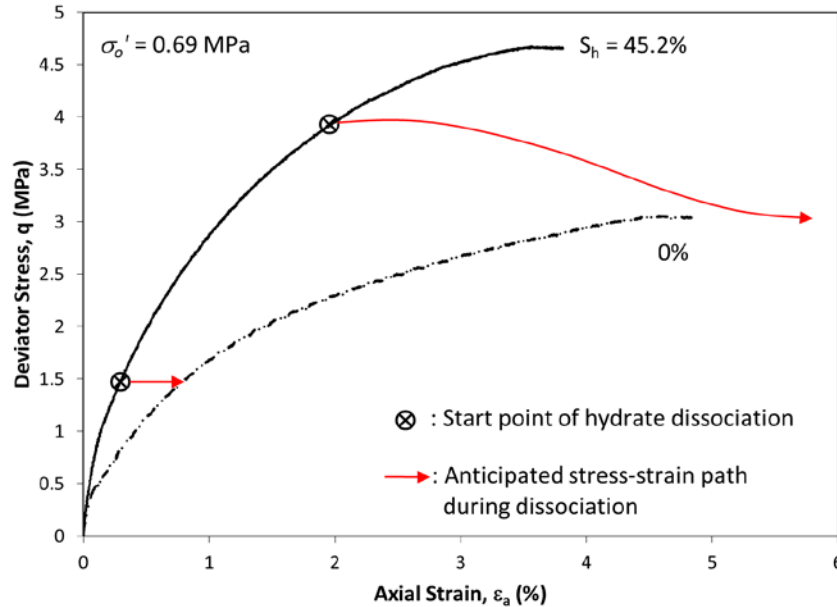


Figure 3: Stress-strain paths during hydrate dissociation anticipated from proposed test plan.

- A plan for minor modification of existing geomechanical test setup is currently being prepared to continuously measure the mass of dissociated methane gas for S_h calculation.
- The test will also be conducted in the upgrading environmental chamber, which can provide better control of temperature (less temperature fluctuation).

Subtask 3.3 Methodology Developments for Modeling Geomechanical Stability of Hydrate-Bearing Sediments under Hydrate Dissociation Condition

Effort has not begun on this subtask; pending supporting research staff emplacement.

Task 4.0 Pore-Scale Visualization and Characterization of Hydrate-Bearing Sediments

Subtask 4.1 Effect of Continuous Brine Flow on Hydrate Formation and Dissociation Behaviors

- Two sets of CT images of hydrate-bearing sediments were obtained. Each set has CT images of sediments before and after hydrate formation (shown in Figures 4 and 5).

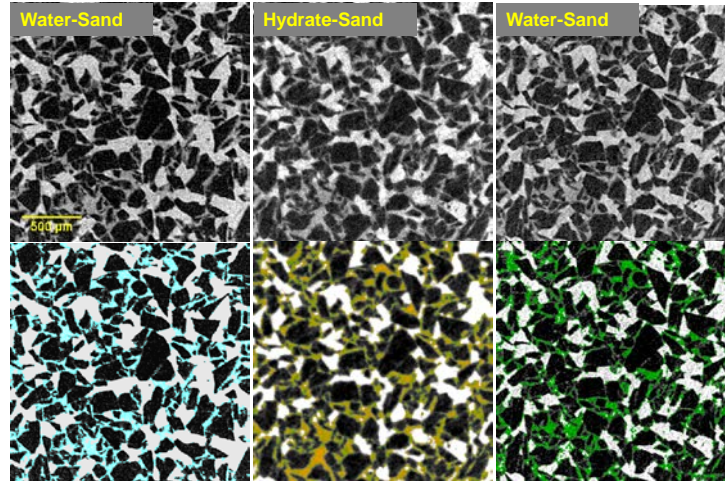


Figure 4: Slice view of partially water saturated sands scanned at (a) atmospheric pressure and room temperature conditions, (b) 7°C and 10MPa gas pressure where water turns into hydrate, and (c) atmospheric and room temperature conditions where hydrate has dissociated and turns back into water.

- Water, gas, and hydrate distributions are being studied at different stages of the experiment.

	(a) Initial condition	(b) Hydrate formation	(c) After hydrate dissociation
Raw CT images			
Colored Water Hydrate			

Figure 5: Methane hydrate synthesized in pure silica sands (grain diameter ~110µm) using the excessive-gas method. (a) Partially water saturated sands are purged by methane gas (to remove air) and scanned at atmospheric pressure and room temperature conditions. (b) Hydrate formation is triggered by lowering the temperature to 7°C and pressuring up to 10MPa. (c) Hydrate dissociation is induced by gradually decreasing the chamber pressure down to atmospheric condition.

Subtask 4.2 Water and Gas Distributions after Hydrate Dissociation and Implications to Permeability

- Pore network simulations of hydrate effects on the relative permeability were completed. The pore networks were extracted from 3D CT images of sands from the Mallik hydrate site (Figure 6).

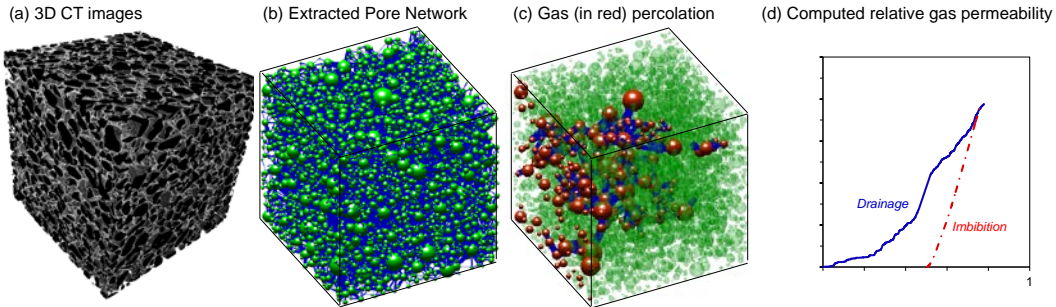


Figure 6: Pore network simulation based on 3D CT images. (a) Obtained 3D CT scanning images of the sands from the Mallik hydrate site. (b) Extracted stick-ball model of the pore network based on the CT images. (c) An illustration of the gas percolation path through the network. (d) Relative gas permeability during the drainage (gas invading water-saturated pore network) and the imbibition (water saturates a dried pore network) processes.

Subtask 4.3 Links between Hydrate Morphologies and Geomechanical Properties

- New endcaps for the Be vessel with capabilities of vertical stress control and wave measurement (to be installed) were designed, machined, and succeeded the leak test (up to 5,500psi) (Figure 7).
- The newly designed endcaps allow vertical effective stress to be applied, while P-wave velocity is measured. Therefore, the hydrate morphology (through CT scanning) will be linked to the geomechanical behavior of hydrate-bearing sediments (small-strain stiffness and large-strain strength).

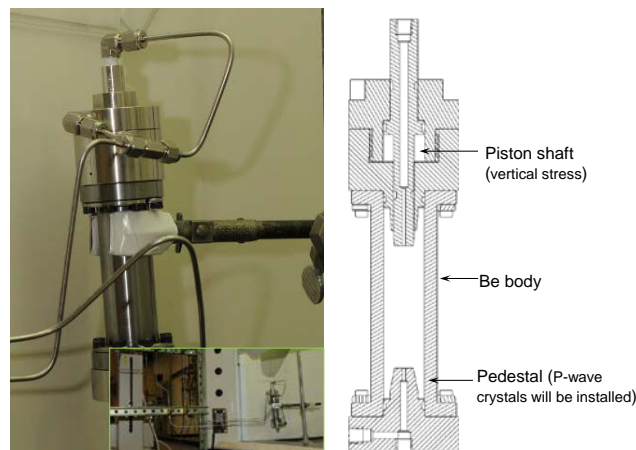


Figure 7: The Be vessel with two new endcaps are under leak test.

Subtask 4.4 Microfluidic-Based Permeability of Hydrate-Bearing Sediments

- The microfluidic chip (purchased from Dolomite Microfluidics) has been flow tested at various differential pressures to determine if it follows Darcy's Law. Testing has shown that Darcy's Law is followed (Figure 8).

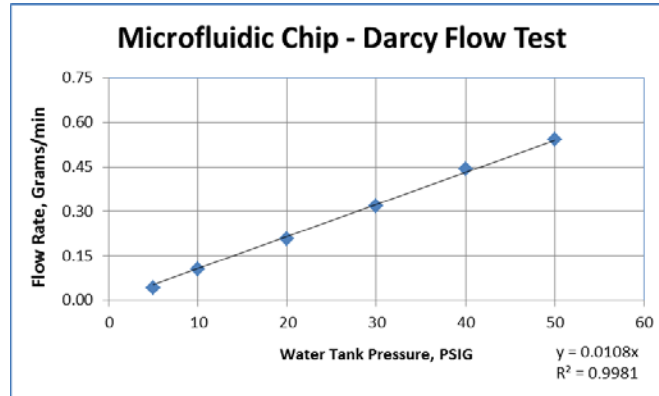


Figure 8: Darcy flow test results.

- The microfluidic chip cooling system was functional and the copper Thermal Transfer Plate (TTP) was machined and was embedded with thermocouples. The cooling system consists of: glycol chiller for system cooling, peltier plates for chilling of the TTP, and proportional-integral-derivative (PID) controllers/Solid-State Relays (SSRs) for control of the peltier plates. The cooling system has been tested and produced the desired linear gradient across the TTP (Figure 9).

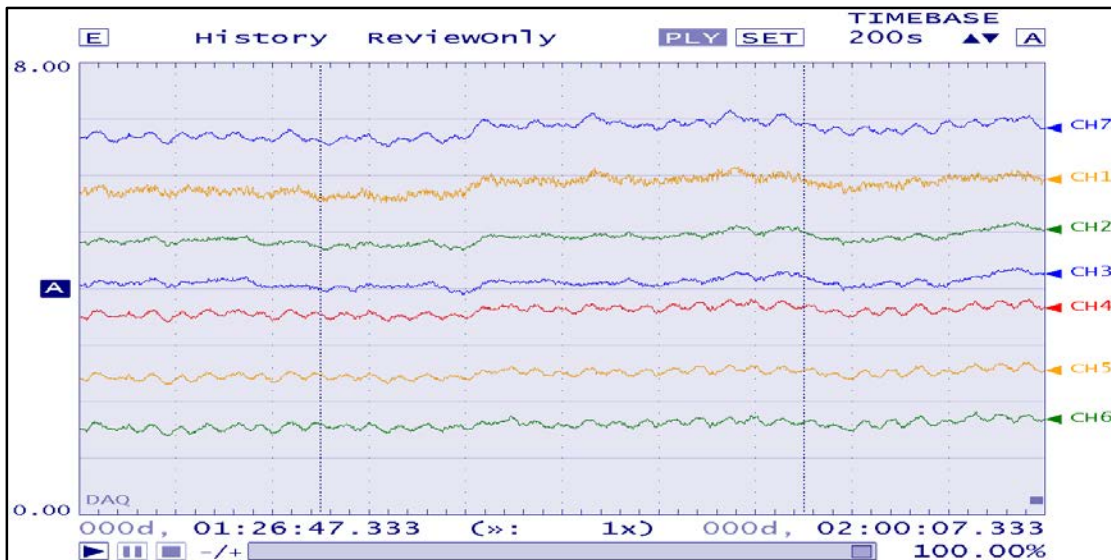


Figure 9: Temperature versus time plot of TTP.

- Additional parts were ordered to make the cooling system more robust. These parts include thermocouples to embed in the peltier plate cooling control and higher-fidelity PID controllers. These parts will be delivered in January 2015 and will be incorporated into the system upon arrival.

- The imaging system is currently functional. This equipment was obtained from WVU Chemical Engineering and has low speed/low definition capability (Figures 10-13). Video and still images can be captured from the imaging system. When the initial experiments are conducted, the quality of the imaging will be tested to determine if it meets the needs for visual characterization of hydrate density. Further upgrades to the imaging system may be needed based on these results.
- Construction of the flow system to deliver the water/ tetrahydrofuran (THF) mixture to the microfluidic chip is underway. For THF experimentation, a high-pressure system is not required. Operating conditions will typically be below 50 pounds per square inch gauge (PSIG). Construction of the flow system is expected to be complete in January 2015.

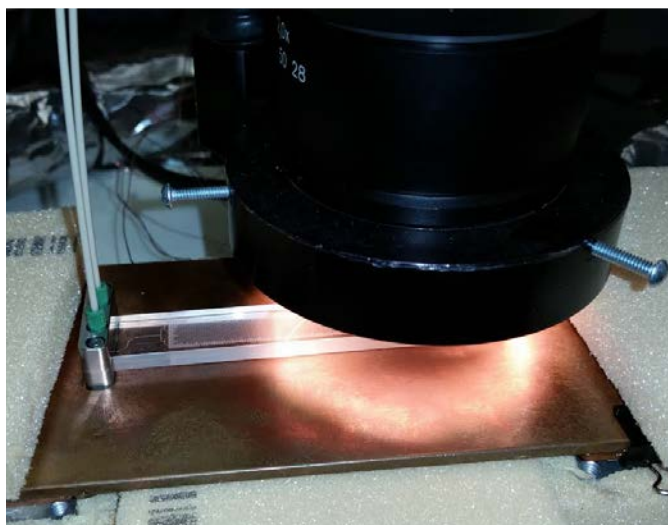


Figure 10: Microfluidic chip on TTP.



Figure 11: Imaging system and chip on TTP.

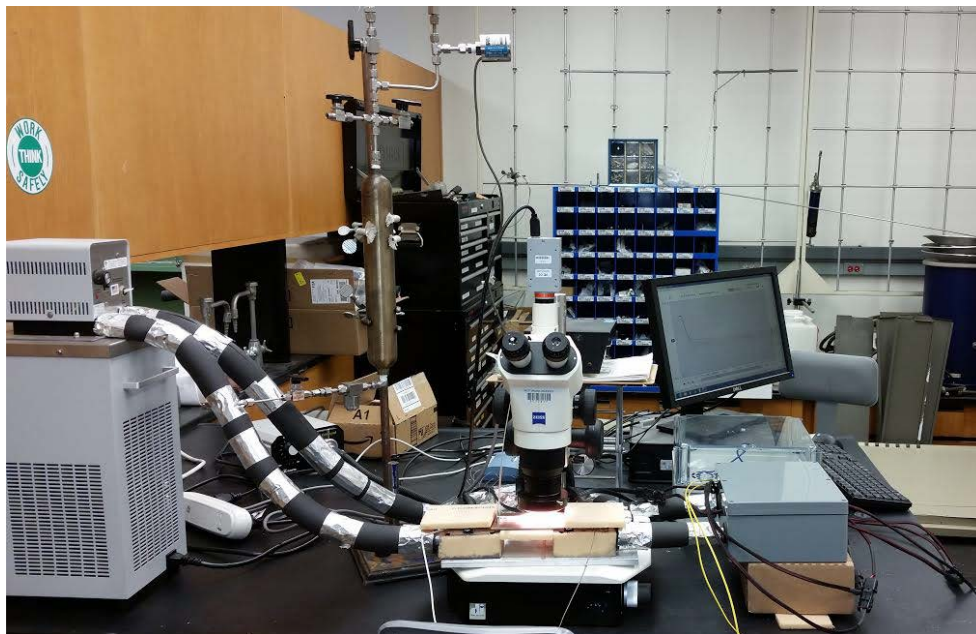


Figure 12: Microfluidic chip system.

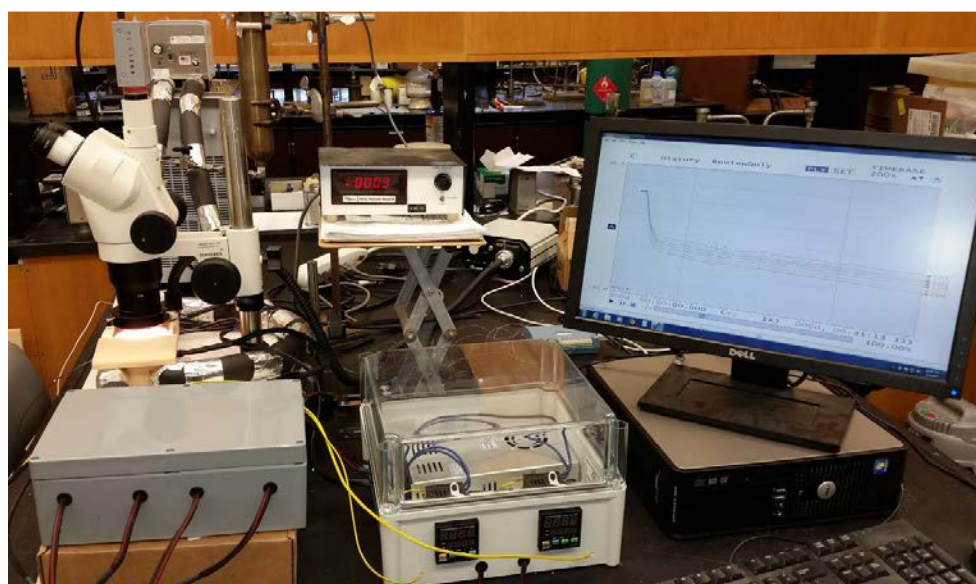


Figure 13: Microfluidic chip system controls.

Forecast for Next 6 Months

Task 1.0 Project Management and Outreach

The FY15-Q1 Report will be submitted on January 30, 2015.

Task 2.0 Reservoir Simulation of Gas Hydrates Production Field Tests

Subtask 2.1 Alaska North Slope Production Test Simulation Assistance

The next six months will involve carrying out uncertainty and sensitivity analyses on both the L-Pad and Mt. Elbert models. Field data will be continuously incorporated into the heterogeneous models as they become available. Also, detailed wellbore design and flow assurance studies will be conducted to forestall problems associated with reformation of hydrates within the wellbore during production. This will involve the application of computational fluid dynamics; its results will be coupled with reservoir models.

Subtask 2.2 International Code Comparison Continuation – Iñnik Sikumi History Match Analysis and Marine Deposit Based on the 2013 Nankai Trough Test or Other Marine Sites

In the next six months, the focus will be on understanding the flow kinetics of the CH₄-CO₂ hydrate considering the injection of CO₂ at the top and bottom of the hydrate stability zones of CH₄ and CO₂ hydrates. The focus will also include conducting simulation scenarios using different production techniques to investigate how the reservoir parameters change for each technique, particularly for the geologic formations with high-hydrate saturations. Focus will change from injecting gaseous CO₂ into different reservoir domains to injecting liquid CO₂ by modifying the Mix3HRS code.

Task 3.0 Laboratory Hydrologic and Geomechanical Characterization and Analysis of Hydrate-Bearing Sediments

Subtask 3.1 Laboratory Measurement of Relative Permeability of CH₄ Gas in Brine-Saturated Hydrate-Bearing Sediments

- The literature review will be continued. (FY15-Q2)
- Development of experimental methodology for the relative measurements will be completed. (FY15-Q2)
- The temperature chamber will be ready for the test by adding new gas lines, temperature controller, and gas detectors. (FY15-Q2)
- New equipment and parts will be assembled into the mobile cart. (FY15-Q2)
- The experimental method and test setup will be examined by conducting preliminary tests. (FY15-Q2)
- The first planned test will be conducted by following completed experimental methodology. (FY15-Q3)

Subtask 3.2 Tri-Axial Compression Tests on Hydrate-Bearing Sediments with Induced Hydrate Dissociation under Shear Stress

- Development of reasonable strategy of hydrate dissociation will be completed in consideration of actual HBS conditions anticipated during field production tests. (FY15-Q2)
- An overall test plan will be completed. (FY15-Q2)

- Modification of the existing geomechanical test setup will be completed in accordance with the test plan. (FY-Q2)
- An initial compression test will be conducted, simultaneously examining the test plan and setups. (FY15-Q3)

Subtask 3.3 Methodology Developments for Modeling Geomechanical Stability of Hydrate-Bearing Sediments under Hydrate Dissociation Condition

Effort has not begun on this subtask; pending identification of research staff on the task. The team hopes to validate the constitutive model with experimental data on the modeling of dissociation on stress-strain behavior. The team would also conduct and develop benchmark tests for validating the coupling analysis for geomechanics analysis of operational scenarios, for use in such cases as methane extraction from the ground.

Task 4.0 Pore-Scale Visualization and Characterization of Hydrate-Bearing Sediments

Subtask 4.1 Effect of Continuous Brine Flow on Hydrate Formation and Dissociation Behaviors

- To follow the NETL's recipe of forming noncementing hydrate and obtain CT images of hydrate pore habits at each critical steps using the Be vessel.

Subtask 4.2 Water and Gas Distributions after Hydrate Dissociation and Implications to Permeability

- To obtain CT images of residual water and gas distributions after hydrate distribution.
- To perform pore network modeling to simulate observed processed and extend the model to other conditions (varying in hydrate saturation, hydrate distribution, pore statistics, etc.) relevant to field conditions.

Subtask 4.3 Links between Hydrate Morphologies and Geomechanical Properties

To use the Be vessel with new endcaps to study the effects of hydrate morphologies on the measured stiffness (i.e., wave velocity) and strength of hydrate-bearing sediments.

Subtask 4.4 Microfluidic-Based Permeability of Hydrate-Bearing Sediments

Beginning in January 2015, experiments with THF hydrate will be conducted to test the system and determine the ability to process images from the experiments. Based on this data, further refinements may be needed to parts of the system to move forward. Image processing will be conducted with ImageJ.

The first experiment will produce THF hydrate in the microfluidic chip without using a temperature gradient. The goal of the experimentation will be to correlate hydrate density to flow, which will show how the permeability of the microfluidic chip changes as hydrate density increases. Once initial testing of THF hydrates are complete, a temperature gradient will be induced to increase the density of hydrate formed, attempting to mimic real world hydrate densities.

Products

Publications, Conference Papers, and Presentations

Dai, S., Seol, Y., and Choi, J.H., “Impacts of Hydrate Pore Habits on the Physical Properties of Hydrate Bearing Sediments,” AGU Fall Meeting Abstracts, 2014, B11B-0011. (Subtask 4.3)

Mahabadi, N., Dai, S., Seol, Y., and Jang, J., “Water Retention Curve and Relative Permeability for Gas Production from Hydrate-Bearing Sediments,” AGU Fall Meeting Abstracts, 2014, B11B-0019. (Subtask 4.2)

Seol, Y., Choi, J.H., Dai, S., and Jarvis, K., “Understanding the Physical Properties of Hydrate Bearing Sediments at Pore- and Core-Scales,” *Fire in the Ice*, under internal review. (Tasks 3.0 and 4.0)

Websites or Other Internet Sites

Hydrate research activity was featured in *Research News*, October 2014, Issue 1, p. 3, “Revealed Secrets in Locked in ICE” and “NETL In-House Research Program: Natural Gas Hydrate R&D” page http://www.netl.doe.gov/File%20Library/Library/Newsroom/researchnews/Research_News_October2014_101514.pdf

Changes/Problems

Deploying the Be vessel for hydrate studies may be delayed, as a result of other projects being behind schedule that engage the Be vessel and the micro-XCT. Aluminum core holders are being designed to be used for Industrial CT (Subtasks 4.1 and 4.3).

On October 17, 2014, our site support contractor, URS Corporation, joined resources with AECOM. They now operate as a single company under the name AECOM. In this document, references to the company address the site support contractor as URS/AECOM.

Fiscal Year 2015 Quarter 2

Accomplishments

Task 1.0 Project Management and Outreach

The FY15-Q2 deliverables included:

- The FY15-Q1 Report was submitted to SCNGO on January 30, 2015.

Task 2.0 Reservoir Simulation of Gas Hydrates Production Field Tests

Subtask 2.1 Alaska North Slope Production Test Simulation Assistance

Accomplishments:

Based on spatial analysis of porosity distribution, a 3D heterogeneous reservoir model was developed.

Objective

The objective for FY15-Q2 was to build a robust reservoir model of the L-pad region based on available field data. During this period, efforts were made towards building a 3D heterogeneous reservoir model of the L-pad C- and D-sands with respect to porosity and hydrate saturation distributions. As a first step, spatial analysis of porosity distribution was conducted using vertical porosity variations derived from up to 78 well logs and by applying geostatistical techniques. Anisotropic variograms of spatial porosity correlations were developed and used to perform stochastic simulations honoring field data. The 3D porosity realizations which resulted were used as input for production simulations of the L-pad reservoir model.

Reservoir Flow Simulation

Preliminary numerical flow simulations were conducted based on a single realization of the heterogeneous porosity distribution. Simulation objectives predict gas and water production rates, ensure that simulations are running problem-free, and (as a second step) apply a geostatistical hydrate distribution based on the experimental porosity-saturation correlations and stochastic residual distributions. A primary goal was to run a set of realizations (possibly quantifying them in respect to the reservoir quality using one or two integrated parameters) to determine ranges of production volumes, to explore the design and operational factors which would affect production, and to recommend production schemes.

Input Field Data

Data used in this study included density logs for wells L-106 and L-112, and volume of shale logs for 78 L-pad wells (including L-106 and L-112). All well log data were provided by USGS.

Methods

The steps taken in this study are outlined (in order) below:

1. Converted density logs of L-106 and L-112 to porosity.
2. Performed correlation of porosity-shale volume using pooled porosity values from L-106 and L-112.
3. Calculated porosity values of the C- and D-sand interval in other 76 wells in the L-Pad region using the porosity-shale volume correlation.

4. Pre-processed data by trimming, declustering, and normalizing the distribution of the well log-derived porosity values.
5. Quantified spatial relationship of porosity by estimating and modeling anisotropic variograms from empirical variograms.
6. Performed ordinary kriging with sequential Gaussian simulation using the modeled variogram as a weighting function to obtain various realizations of porosity distribution
7. Conducted preliminary reservoir flow simulation on a single realization.

Software

Geostatistics: WinGSLIB v.1.5.6 (Full Version)

Reservoir Flow Simulation: CMG STARS 2014

Density to Porosity Conversion

Conversion of density to porosity in wells L-106 and L-112 were completed using the following relations (Crain, 2015):

$$\varphi = \frac{\rho - \rho_m}{\rho_w - \rho_m}, \quad \varphi_{sh} = \frac{\rho_{sh} - \rho_m}{\rho_w - \rho_m}, \quad \varphi_c = \varphi - \varphi_{sh}V_{sh}$$

ρ = density log value

ρ_m = matrix rock density = 2.65

ρ_w = density of water = 1.00

ρ_{sh} = shale density \cong 2.37

φ = porosity without correction

φ_{sh} = shale porosity correction

φ_c = shale – corrected porosity

V_{sh} = volume of shale from log

Porosity-Shale Volume Correlation

A porosity-shale volume relationship was developed from porosity values pooled from wells L-106 and L-112 as shown in **Error! Reference source not found.**

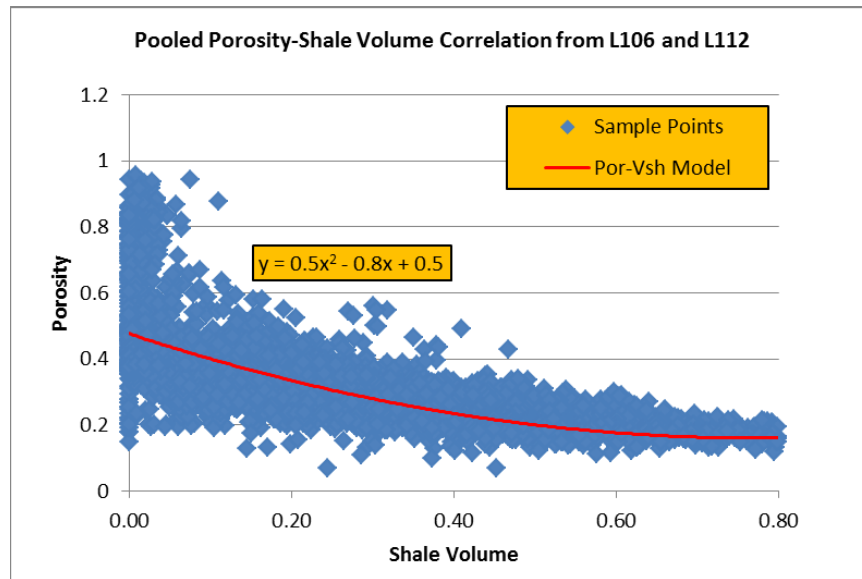


Figure 14: Pooled correlation from L-106 and L-112 well logs.

Error! Reference source not found. shows that there is quite a close agreement between the above correlation with that of Collett et al., 2012. The discrepancy arises because Collett et al., 2012 used the whole shale volume (Vsh) range, while the range was limited to 0 – 0.4, constituting more than 80% of the total shale volume measurements and falling within depths of 110 – 2,800 ft.

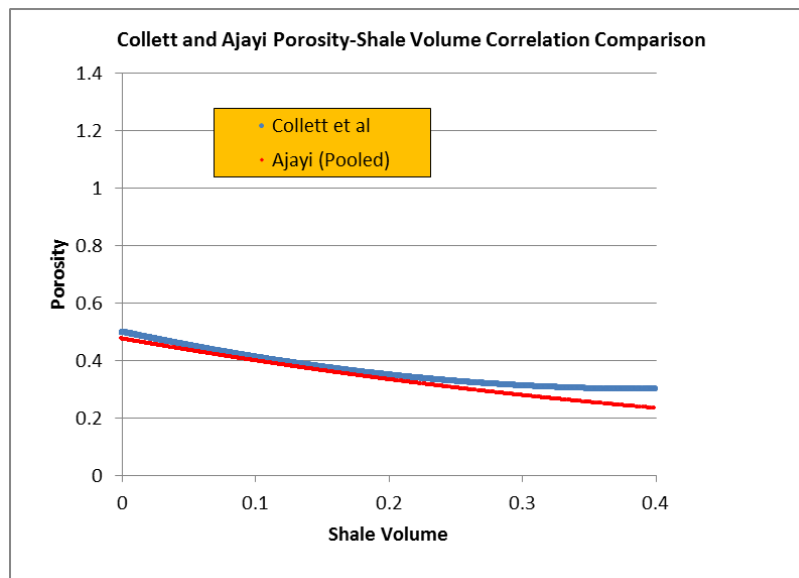


Figure 15: Comparison of porosity-shale volume correlations.

Estimation of Porosity Values in other Wells

The validated correlation was used to estimate the porosity values from the Vsh of the remaining 76 wells in the depth range of 646 – 723 m (C-sand interval). Estimated porosity values from a total of 78 wells will represent “sampled” (or “known”) porosity input data that will be used to obtain geostatistical realizations of porosity distributions in the whole reservoir volume.

Error! Reference source not found. shows a relative frequency histogram of the estimated porosity values with a mean of 0.36, standard deviation of 0.07, and in the range 0.18 – 0.50.

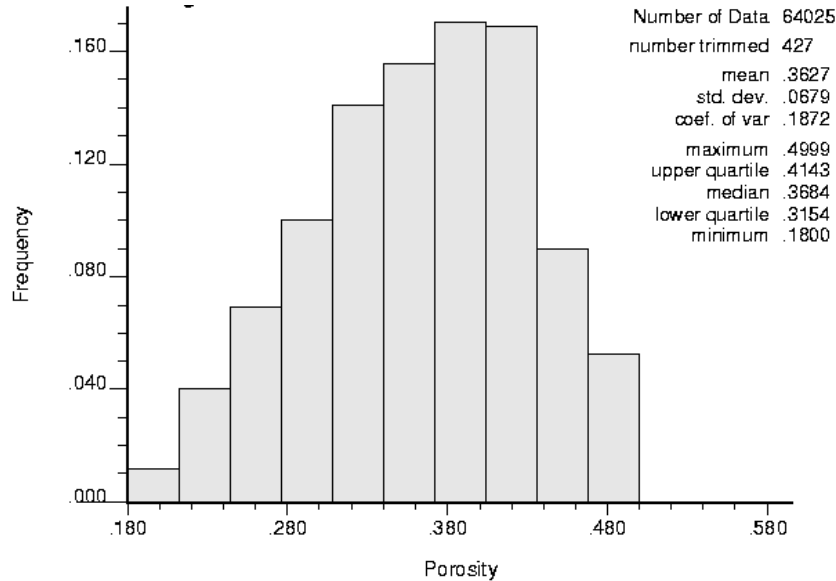


Figure 16: Relative frequency histogram of well log-derived porosity data.

Data Pre-Processing

Trimming

The well log-derived porosity values within the C-sand interval were trimmed to be within the range 0.20 – 0.45 which represents about 80% of the original distribution. Trimming was necessary to reduce the variability of the hydrate-bearing sand porosity, because significant porosity fluctuations at adjacent reservoir areas might lead to computational convergence problems.

Declustering

The porosity data represent about 64,000 data points in a region with acreage of 1,200 x 1,200 m and depth of 77 m (C-sand) + 40 m (D-sand). **Error! Reference source not found.** shows a gridded surface location map of the intersection of the L-pad wells with the top of the C-sand. It reveals some “clustering” nature of the well positions/porosity data in the x-y plane.

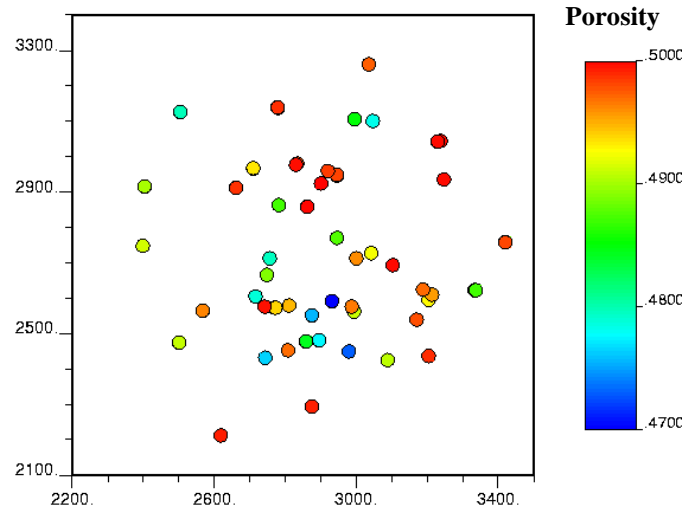


Figure 17: Location map of wells showing porosities of the top-most layer.

Clustering introduces some “bias” in the distribution; therefore, in an attempt to remove bias, a cell declustering technique was used. By varying the cell sizes, a “declustered” mean was calculated using the equation:

$$\bar{x} = \sum_{i=1}^n w_i x_i$$

The weight, w_i , is the reciprocal of the number of sample points in a particular cell for a given cell size. The declustered mean was calculated and plotted for each cell size and the cell size with minimum declustered mean of 0.338 was selected as illustrated in **Error! Reference source not found.**

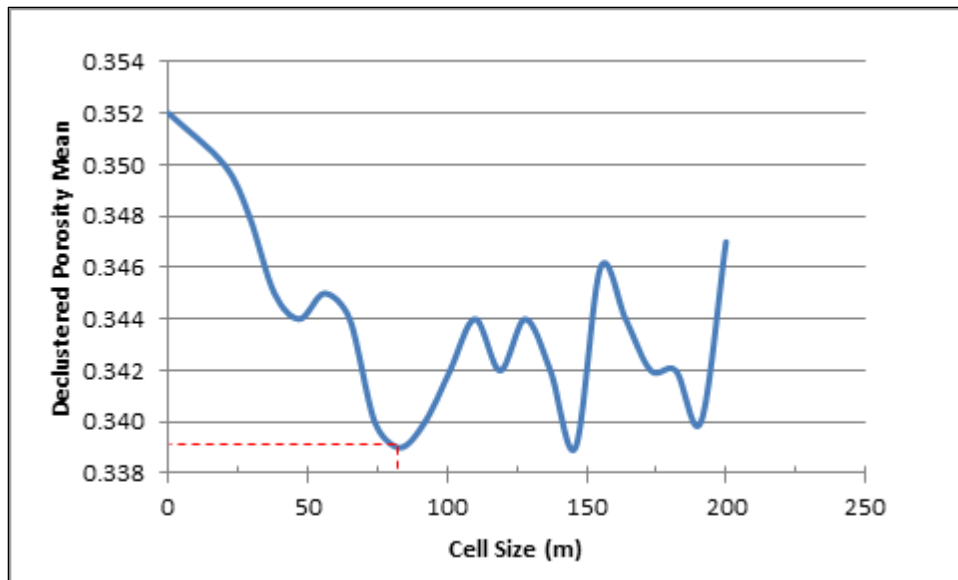


Figure 18: Cell declustering of porosity distribution.

A new relative histogram for the declustered distribution is plotted and shown in **Error! Reference source not found.**

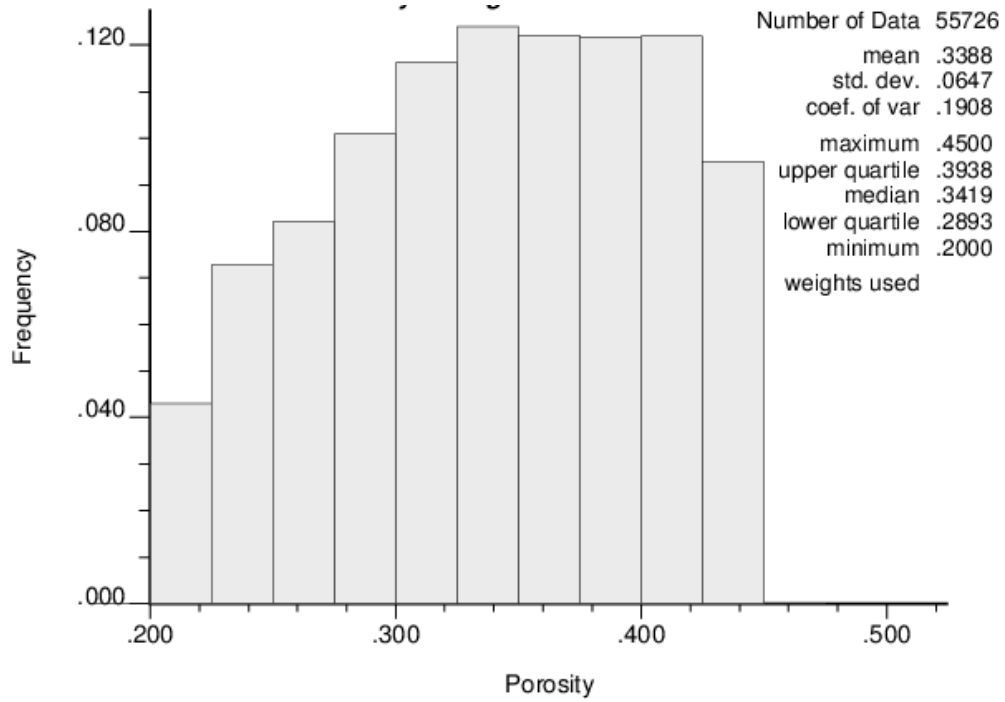


Figure 19: Relative histogram of declustered porosity distribution.

The declustered porosity distribution is shown to have a mean of 0.34 which is lower than the original distribution mean. Using a normal score transformation, the porosity distribution was normalized and is shown in **Error! Reference source not found.**

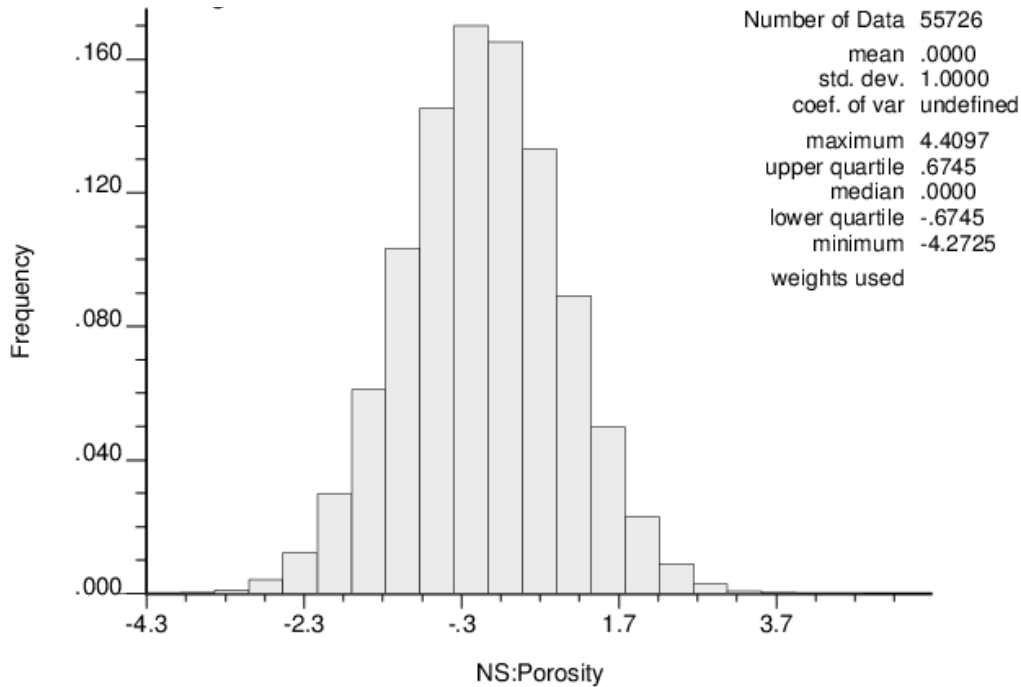


Figure 20: Relative frequency histogram of normalized declustered porosity.

Variogram Estimation and Modelling

Variogram Definition

The variogram is a measure of the variability of a quantity sampled in different locations with respect to spatial coordinates. It is a function of both distance and direction and mathematically defined as:

$$\gamma(\mathbf{h}) = \frac{1}{2N(\mathbf{h})} \sum_{i=1}^{N(\mathbf{h})} [z(\mathbf{x}_i) - z(\mathbf{x}_i + \mathbf{h})]^2$$

where,

\mathbf{h} = displacement vector between a pair of samples (lag distance)

$N(\mathbf{h})$ = Number of sample pairs separated by \mathbf{h}

\mathbf{x}_i = position vector of one of the i^{th} sample pair

$z(\mathbf{x}_i)$ = sampled quantity with position vector \mathbf{x}_i

$\gamma(\mathbf{h})$ = Variogram of any two sample pairs separated by \mathbf{h}

Anisotropic Variograms

The next step was to estimate variograms in the principal directions, i.e., directions of maximum and minimum geological continuity. Two angles define a variogram direction: (1) the azimuth angle (ϕ) and (2) the dip angle (θ), as illustrated in **Error! Reference source not found.** The geology of the ANS suggests that the direction of deposition is along its dip, about 2.3° downwards from the horizontal, which is an approximate direction of maximum geological continuity (hereby called the “horizontal” direction).

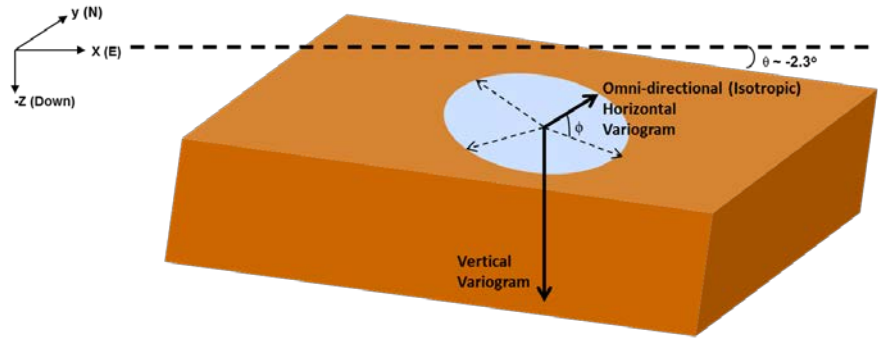


Figure 21: Anisotropic variograms with dip and azimuth angles.

An isotropic horizontal variogram was estimated by using a large azimuthal angle tolerance of $\pm 80^\circ$. A horizontal lag distance of 104 m was used based on the intervals of the peaks of the histogram of horizontal distances between wells shown in **Error! Reference source not found.** This would guarantee a maximum number of sample pairs when estimating the variogram at each lag distance.

The vertical variogram was calculated with a dip = -90° and a vertical lag distance of 2 m given more dense input porosity values in the vertical direction (0.5 ft).

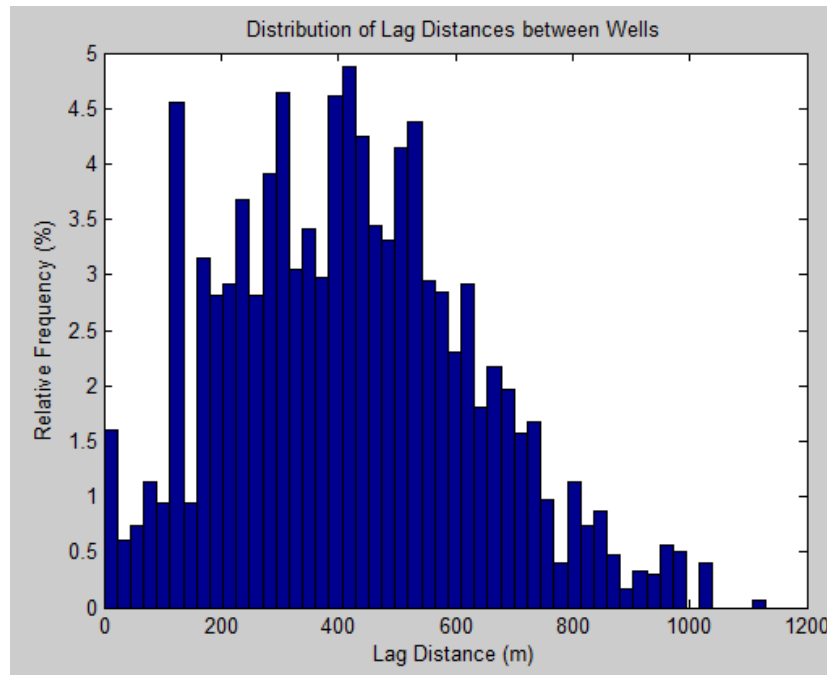


Figure 22: Relative frequency histogram of “horizontal” lag distances between wells.

Plots of the experimental horizontal and vertical variograms and their models are shown in **Error! Reference source not found.** and **Error! Reference source not found.**, respectively. The variograms are standardized and each has a sill of 1.0. A sill is the plateau of variogram plot (theoretically equal to the variance without standardization) while the range is the lag distance at which the variogram reaches the sill. The variogram function is obtained by fitting models to the

horizontal and vertical experimental variograms simultaneously. The variogram model is typically a superposition of two or more standard models which will be discussed shortly.

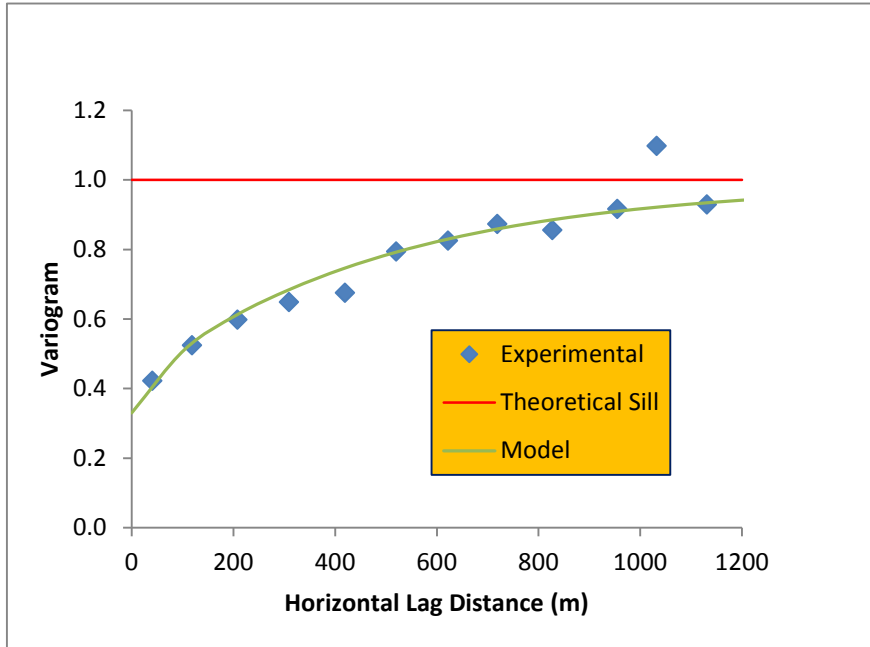


Figure 23: Experimental horizontal variogram and model.

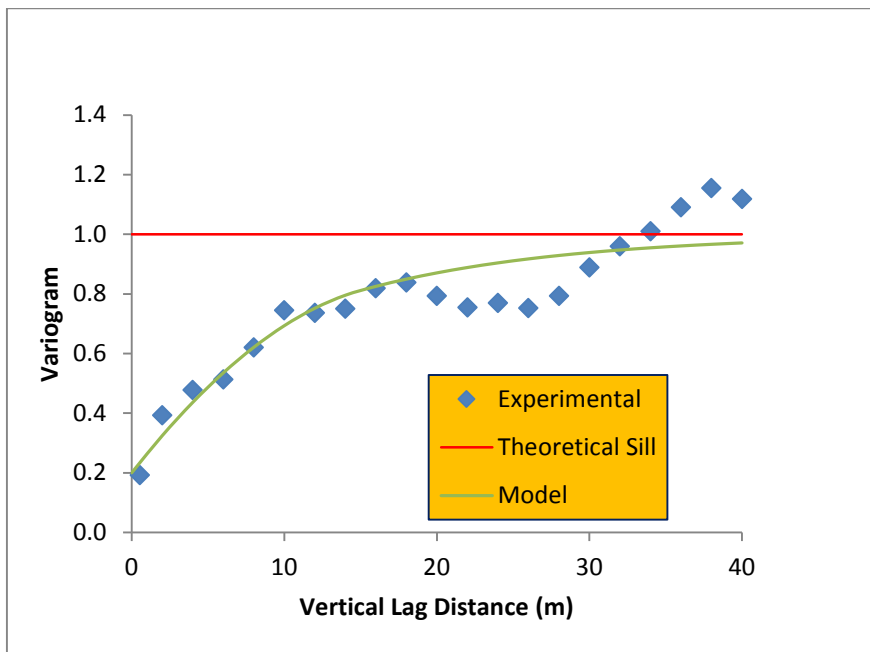


Figure 24: Experimental vertical variogram and model.

Error! Reference source not found. shows the parameters of the final variogram model for this study.

Table 2: Variogram Model Parameters

Model Type	Variance Contribution	Horizontal Range, a_{hor} (m)	Vertical Range, a_{vert} (m)
Nugget	0.2	-	-
Exponential (1)	0.58	1450	40
Spherical (2)	0.08	150	∞
Spherical (3)	0.13	1	∞
Spherical (4)	0.10	∞	15

The variogram function is mathematically expressed as:

$$\begin{aligned} \gamma(h) = & 0.2 + 0.58(1 - e^{-3h_1}) + 0.08 \times \begin{cases} [1.5h_2 - 0.5h_2^3], & \text{if } h_2 \leq 1 \\ 1, & \text{if } h_2 \geq 1 \end{cases} \\ & + 0.13 \times \begin{cases} [1.5h_3 - 0.5h_3^3], & \text{if } h_3 \leq 1 \\ 1, & \text{if } h_3 \geq 1 \end{cases} \\ & + 0.10 \times \begin{cases} [1.5h_4 - 0.5h_4^3], & \text{if } h_4 \leq 1 \\ 1, & \text{if } h_4 \geq 1 \end{cases} \end{aligned}$$

Where,

$$h_i = \sqrt{\left(\frac{h_{vert}}{a_{vert_i}}\right)^2 + \left(\frac{h_{hor}}{a_{hor_i}}\right)^2}, i = 1, 2, 3, 4$$

and

- h_{vert} = distance between sampled and unsampled points in the vertical direction
- h_{hor} = distance between sampled and unsampled points in the horizontal direction
- a_{vert} = variogram range in the vertical direction
- a_{hor} = variogram range in the horizontal direction

The first term (0.2) is nugget effect which represents a discontinuity at zero lag distance. It reflects the independence of the porosity distribution with spatial coordinates.

The second term is an exponential model with a variance contribution of 0.58 and horizontal and vertical ranges of 1,450 m and 40 m, respectively. The third term is a spherical model with a variance contribution of 0.08 and horizontal range of 150 m, and so on.

The longer the range of variogram is in a particular direction, the less the variance contribution in that direction. To obtain variograms for all intermediate angles between the vertical and the horizontal, the lag distance vector is decomposed to h_{vert} and h_{hor} , and then the h_i 's are evaluated.

Stochastic Simulation

Using the variogram as weighting functions, *Ordinary Kriging* along with *Sequential Gaussian Simulation* was performed on a rectangular reservoir grid of 50 x 50 x 200 cells with the size of 25 x 25 x 0.4 m each in the x, y, and z directions, respectively. *Sequential Gaussian Simulation* ensures that the location of the sample data honor their original values (unlike the case if only *Ordinary Kriging* was used).

A search ellipsoid with radius of 300 m and depth of 2 m was used. The search was restricted to a maximum of eight nearest points. The output, which is the normal score porosity, was transformed back to actual porosity values populating the simulation inclined grid by means of a code generated in MATLAB .

Results

Horizontal cross sections of porosity distribution for selected layers are shown in **Error! Reference source not found.** These were obtained for a single realization.

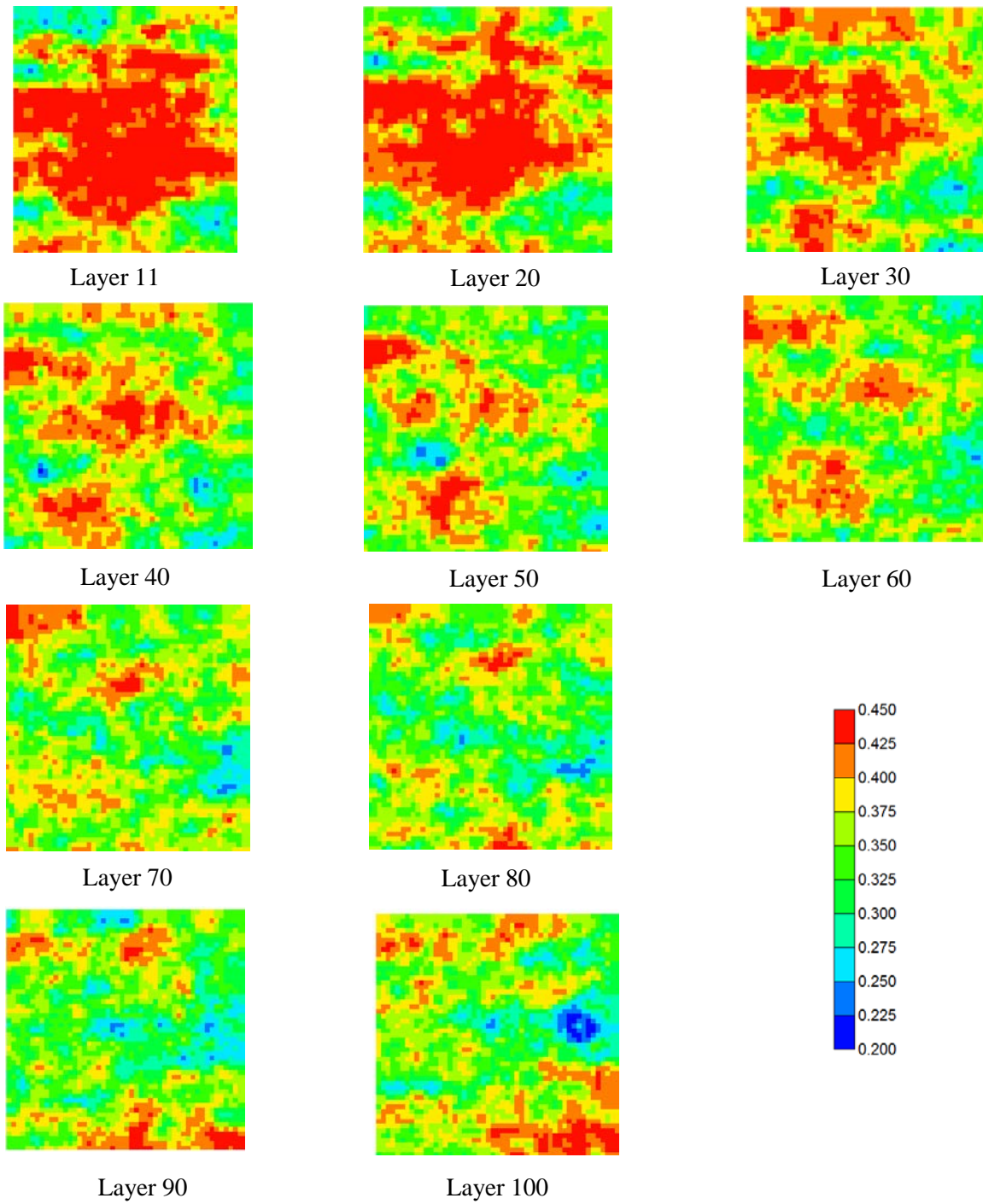


Figure 25: Horizontal cross sections of porosity distribution.

Selected vertical cross sections of porosity distribution are shown in **Error! Reference source not found.**

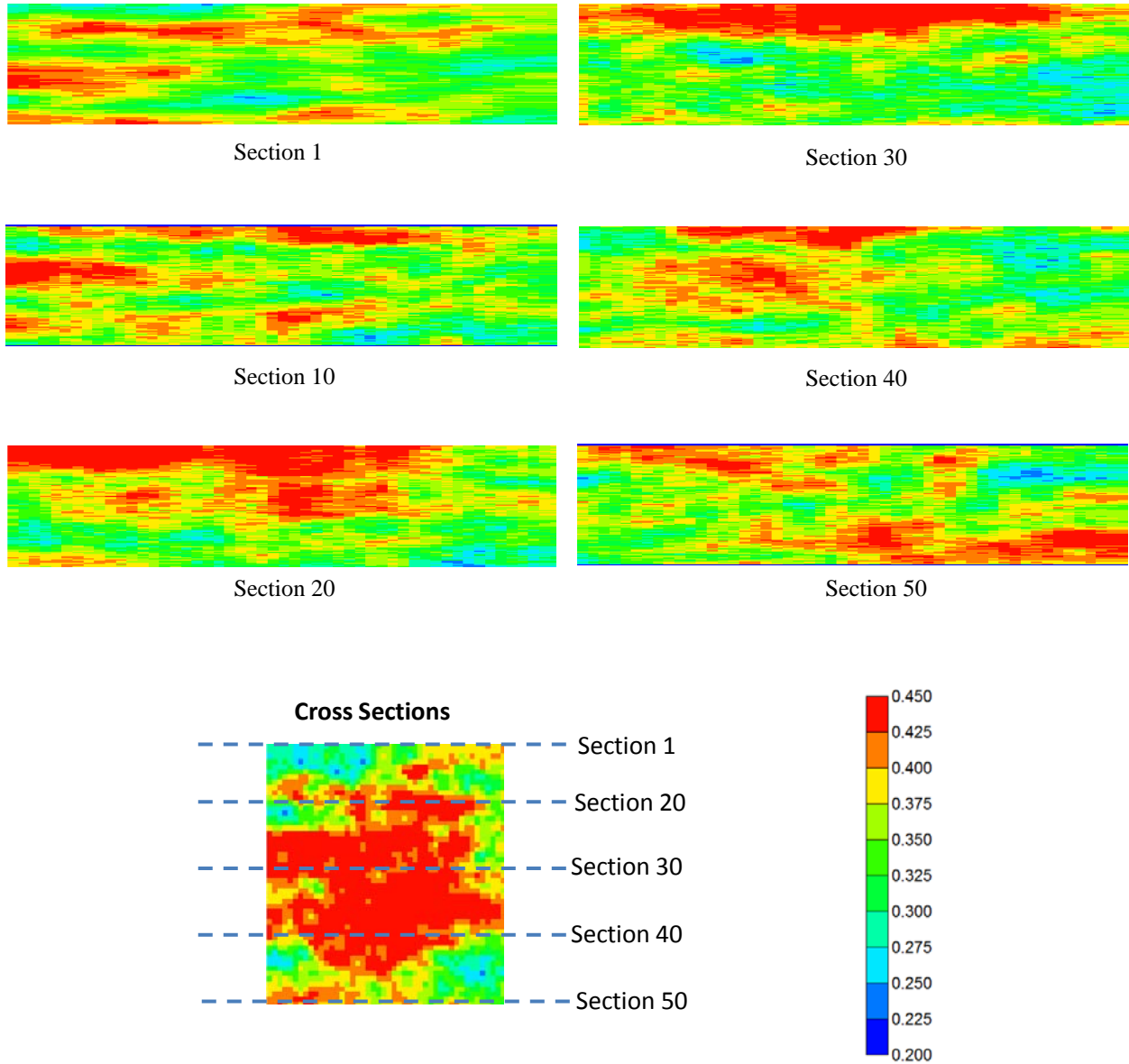


Figure 26: Vertical cross sections of porosity distribution.

A 3D reservoir model, with overburden and underburden low-permeability shale layers, is shown in **Error! Reference source not found.**

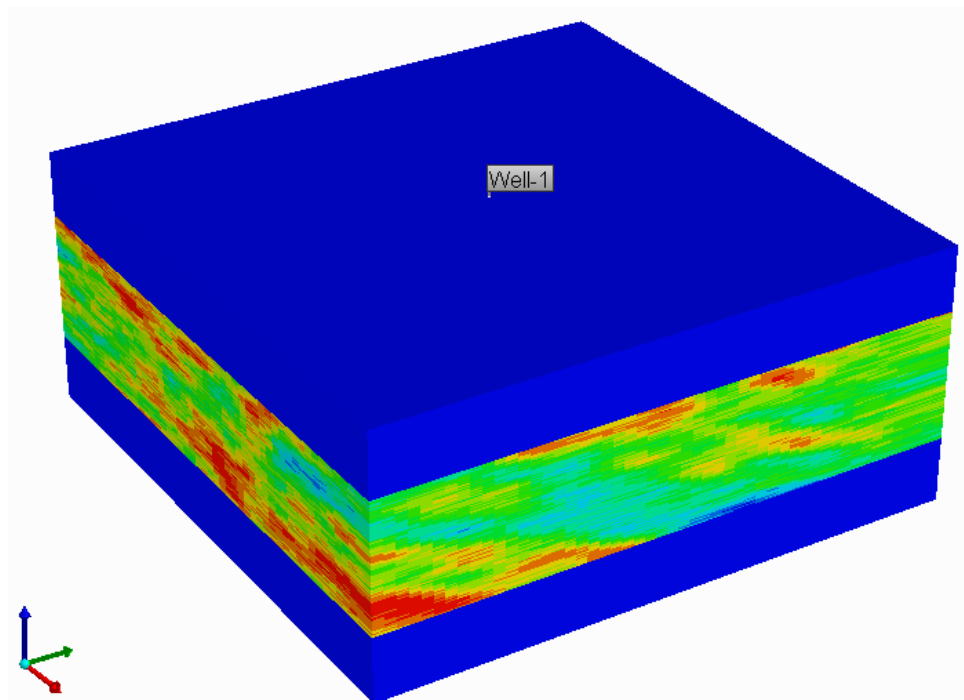


Figure 27: 3D reservoir model.

References

Collett, T.S., Boswell, R., Lee, M.W., Anderson, B.J., Rose, K., and Lewis, K.A., “Evaluation of Long-Term Gas-Hydrate-Production Testing Locations on the Alaska North Slope,” 02, s.l. : Society of Petroleum Engineers, SPE Reservoir Evaluation & Engineering, Vol. 15, pp. 243-264, April 2012.

Crain, E.R. “Porosity from Density Log Model,” *Crain's Petrophysical Handbook*. [Online] 2015 <https://www.spec2000.net/12-phidn.htm>.

Subtask 2.2 International Code Comparison Continuation – Iñnik Sikumi History Match Analysis and Marine Deposit Based on the 2013 Nankai Trough Test or Other Marine Sites

Accomplishments:

- A Class 2 inclined homogeneous methane hydrate reservoir was developed and CO₂ injection as a new gas production method was simulated.

Activities Accomplished This Period

A Class 2 inclined homogeneous methane hydrate reservoir model was developed based on the P/T conditions that existed at the L-Pad. The sand, fully saturated with water underneath the hydrate zone, is known to cause gas production deterioration due to a significant amount of water produced. The CO₂ injection stage into water formation below hydrate-water contact boundary allows the formation of CO₂-hydrate at the depth beneath 2248 ft (685 m). The CO₂-hydrate formation reduces the amount of mobile water in the reservoir and facilitates methane production during the next stage of the CH₄-hydrate depressurization. The approach offers a possibility to permanently store carbon dioxide in the underground formation and by doing so, enhances

methane production from the gas hydrate lying above. Different cases are considered which are intended to provide increased hydrate formation during the injection stage, thus enhancing the impermeability of the lower part of the domain.

Case 1:

In this case, the injection of $\text{CO}_2(\text{g})$ is considered in Zone 2 for 10 days to allow the CO_2 -hydrate formation in the reservoir as shown in **Error! Reference source not found.**

Initial conditions:

- Zone-1 is considered as pure CH_4 -hydrate with coexisting aqueous and hydrate phase ($S_{\text{aq}}=0.5$ and $S_{\text{H}}=0.5$) at 6.5MPa and 5°C .
- Zone 2 was considered as sand (pure aqueous phase ($S_{\text{aq}}=1.0$)) 6.8 MPa and 5.5°C .
- The injection well is modeled as a fixed boundary condition with gas phase at 8.5 MPa and $T = 5^\circ\text{C}$ and for production phase, fixed state boundary was maintained at the production well at bottom-hole pressure of 3.5 MPa and $T = 5^\circ\text{C}$.

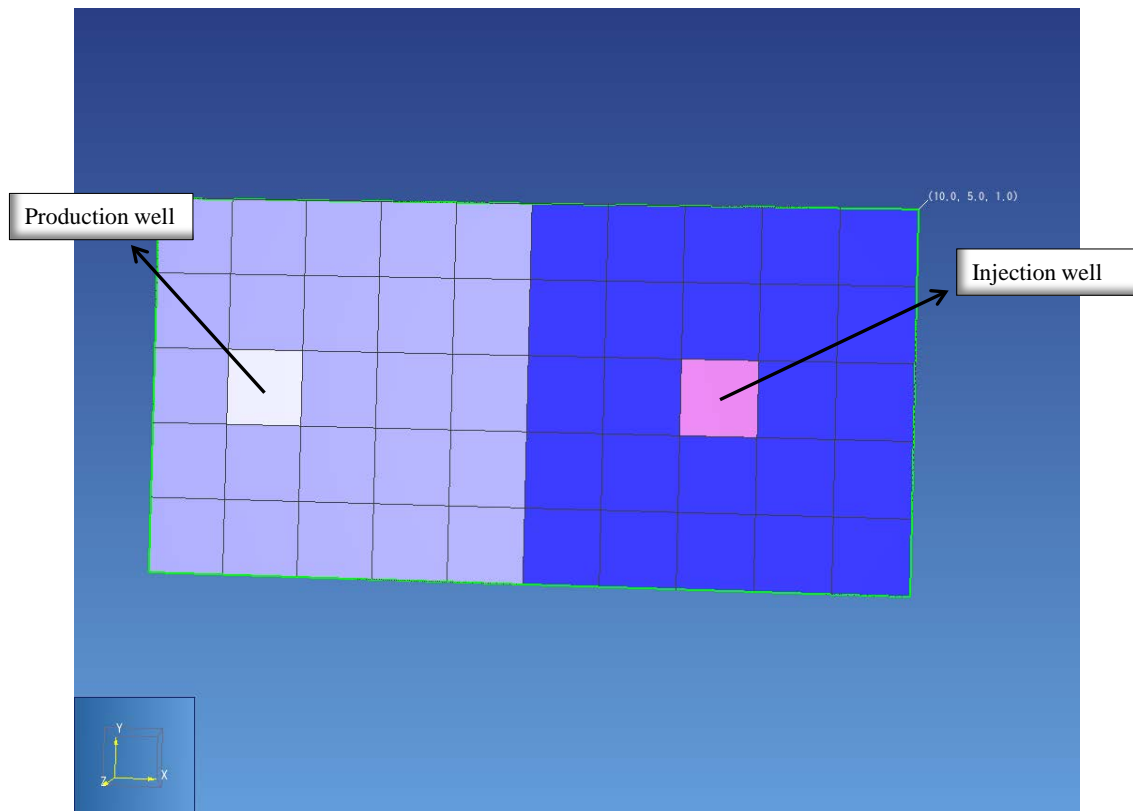


Figure 28: An inclined reservoir domain used in this simulation (side view).

The simulation is performed in three steps (shown in **Error! Reference source not found.**).

Step 1 – Initially, injection of CO_2 is done for 10 days and then the domain is depressurized for 30 days.

Step 2 – Followed by injection of $\text{CO}_2(\text{g})$ for 20 days and depressurization for 60 days.

Step 3 – Finally domain is again pressurized by injecting CO₂ for 20 days and depressurized for 120 days.

Results and Discussion:

Injection Phase:

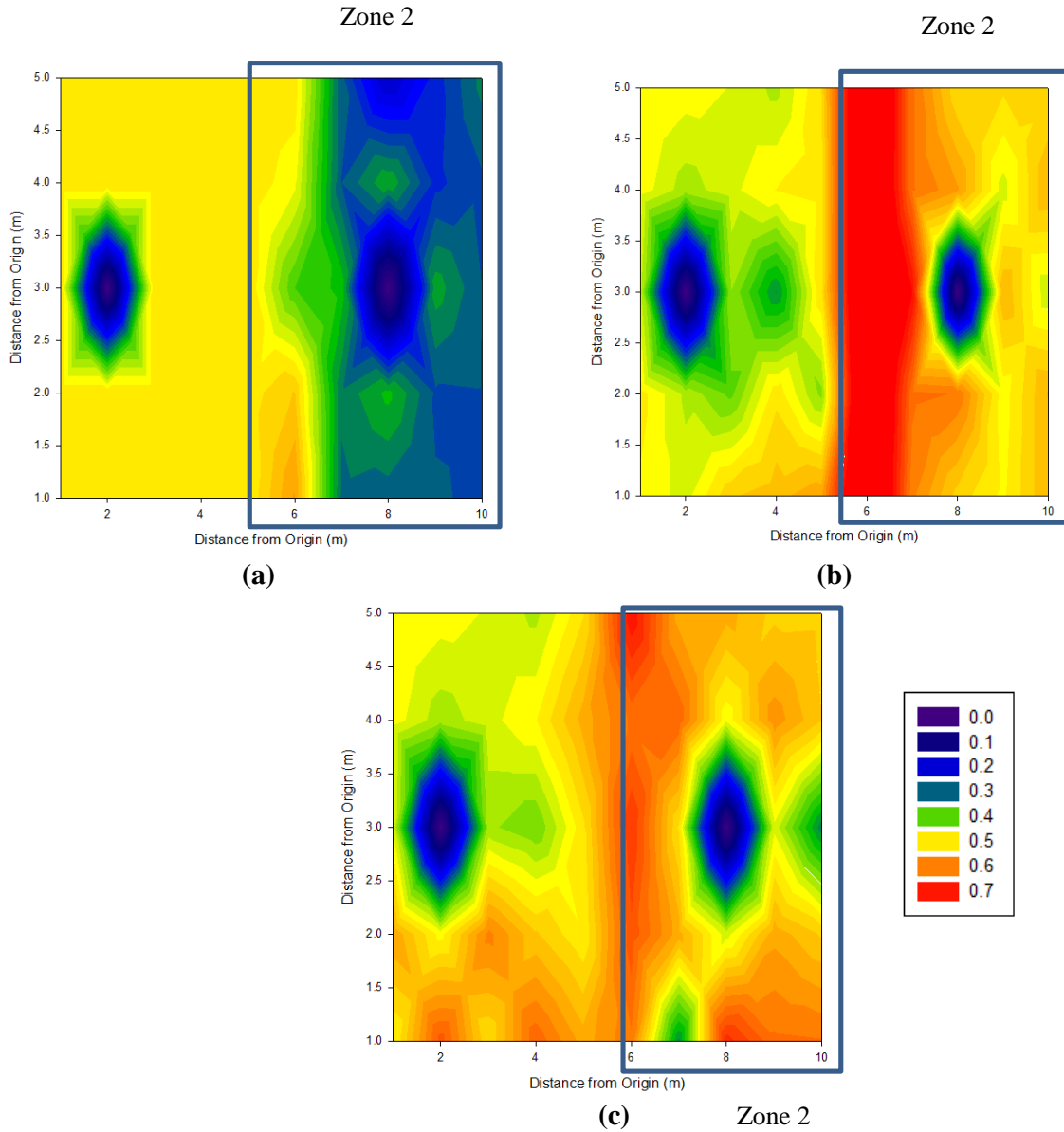


Figure 29: Hydrate saturation profiles at the end of (a) Step 1 Injection, (b) Step 2 Injection, and (c) Step 3 Injection.

From the above contours, it is clear that upon the injection, at the end of each step, the hydrate saturation of Zone 2 increased significantly.

Error! Reference source not found. shows that the amount of water produced decreased significantly from Step 1 to 3. That is a direct consequence of increased saturation in the carbon dioxide hydrate in the domain (Zone 2) that reduces the mobile water available for production.

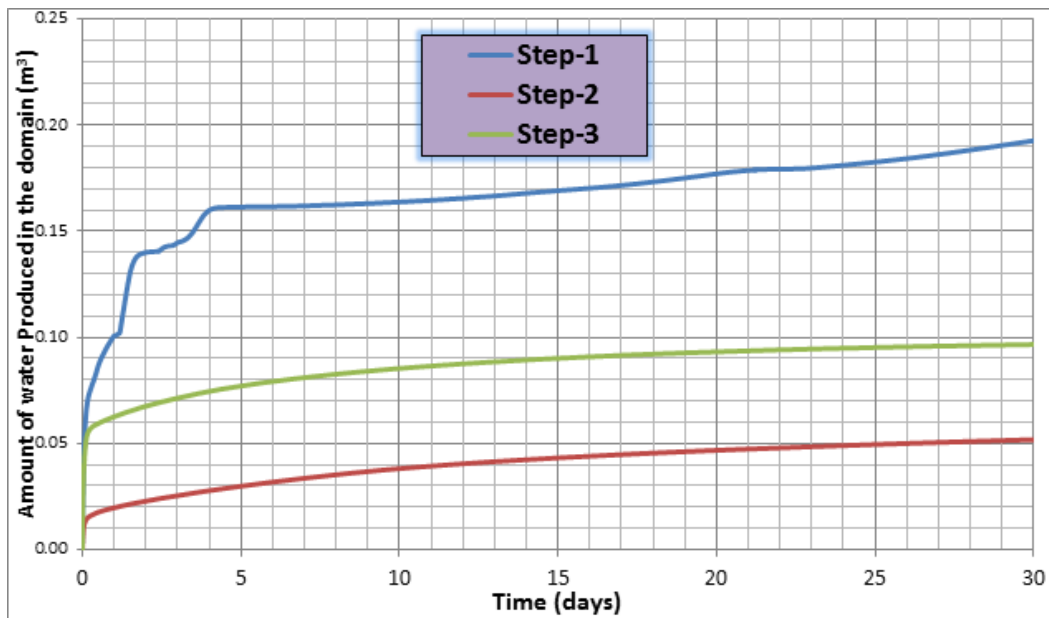


Figure 30: Amount of water produced after depressurization of each step.

Case 2:

Domain Description:

The reservoir domain is 20 m thick and 50 m long (as shown in **Error! Reference source not found.**). Inclination of the domain is 5°. The reservoir domain is considered as two different zones, Zone 1 being CH₄-Hydrate and Zone 2 (below 685 m) as Sand ($S_{aq}=1$).

Initial conditions:

- Zone 1 was considered as pure CH₄-Hydrate with coexisting aqueous and hydrate phase ($S_{aq}=0.5$ and $S_H=0.5$) at an average 6.5MPa and 3.5°C.
- Zone 2 was considered as sand (pure aqueous phase ($S_{aq}=1.0$)) at an average 6.8 MPa and 4.3°C.
- The injection well is modeled as a fixed boundary condition with gas phase at 9.5MPa and 5°C; for the production stage, fixed state boundary was maintained at the production well at bottom-hole pressure of 3.5MPa and 5°C.

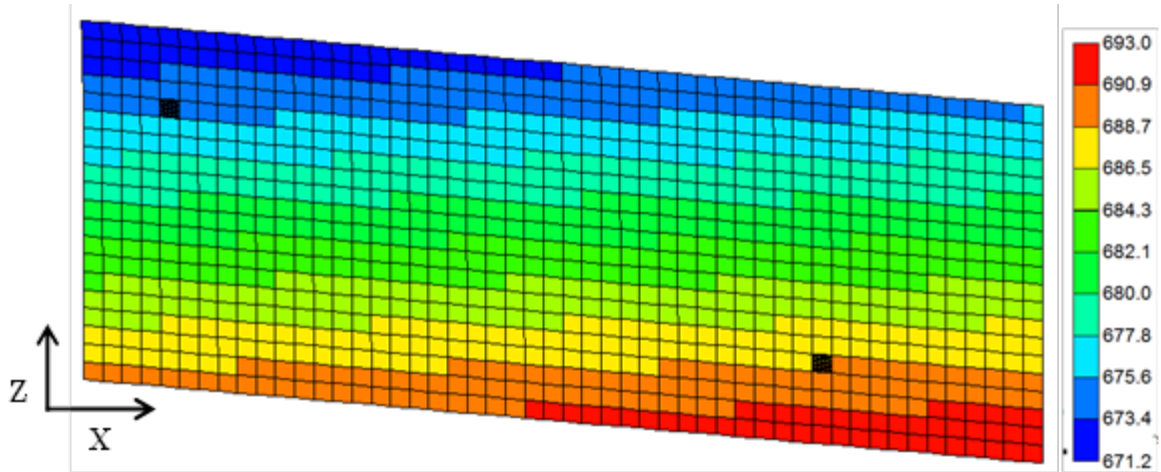


Figure 31: An inclined reservoir domain used in this Case 2 simulation (side view).

The simulation is performed in two steps.

Step 1 – Initially, injection of CO₂ is done in an attempt to convert the entire water-saturated sand region into a hydrate region and then depressurize the domain.

Table 3: Variables used in this Case 2 simulation

Parameters	Value Used
Porosity	0.3
Density	02650 Kg/m3
Thermal Conductivity	2.0 W/m K
Specific heat	750 J/kg K
Pore Compressibility	5.0×10-10 Pa-1
Permeability of the domain	1000 mD

Initial conditions of the domain (**Error! Reference source not found.** and **Error! Reference source not found.**):

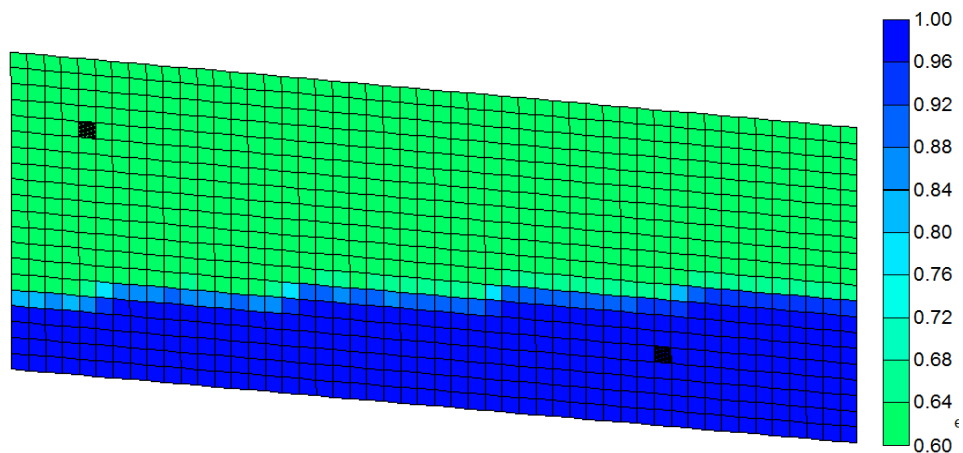


Figure 32: Initial aqueous saturation of the domain.

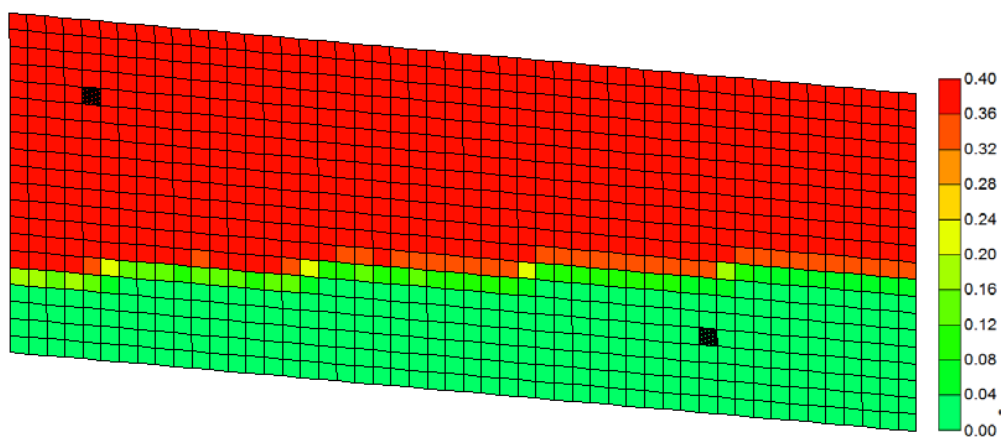


Figure 33: Initial hydrate saturation of the domain.

Results:

Distributions of temperature (**Error! Reference source not found.**), pressure (**Error! Reference source not found.**), saturations of hydrate (**Error! Reference source not found.**), water (**Error!**

Reference source not found.), and gas (Error! Reference source not found.) at the end of 800 days of injection are shown below:

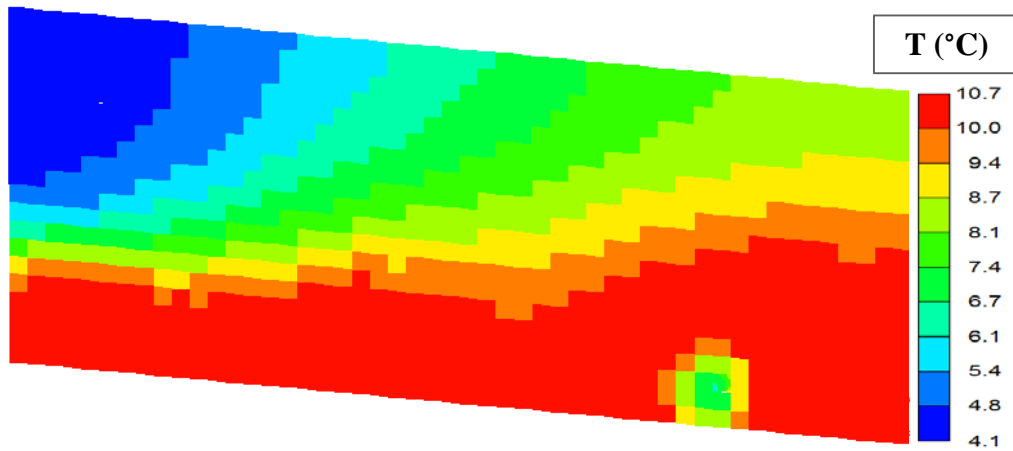


Figure 34: Temperature distribution in the domain.

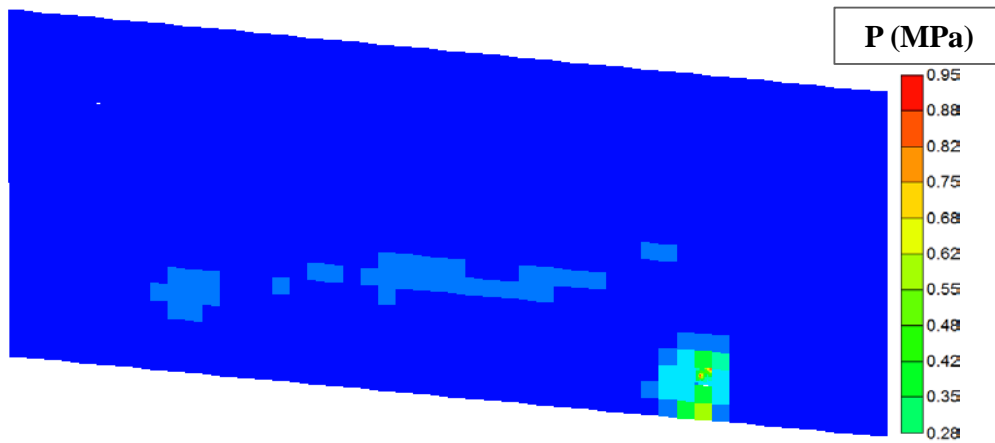


Figure 35: Pressure distribution in the domain.

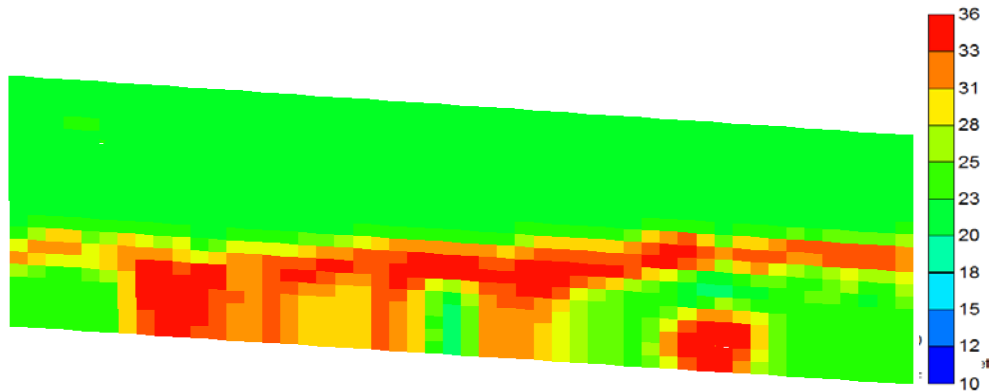


Figure 36: Hydrate saturation distribution in the domain.

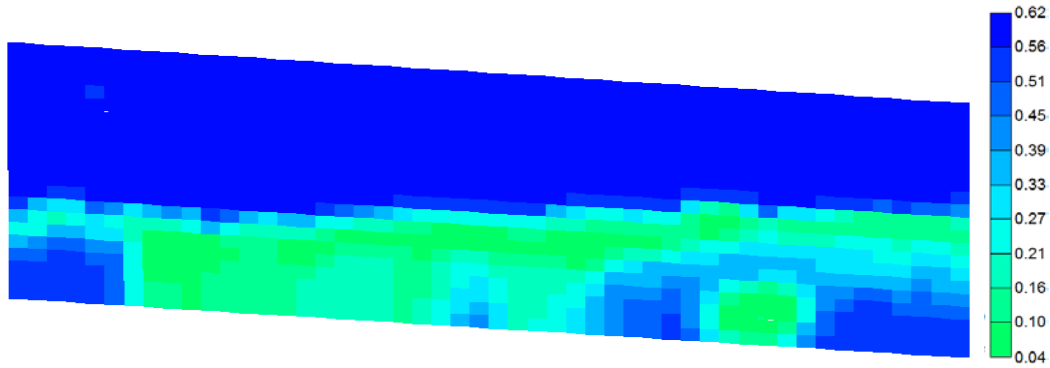


Figure 37: Aqueous saturation distribution in the domain.

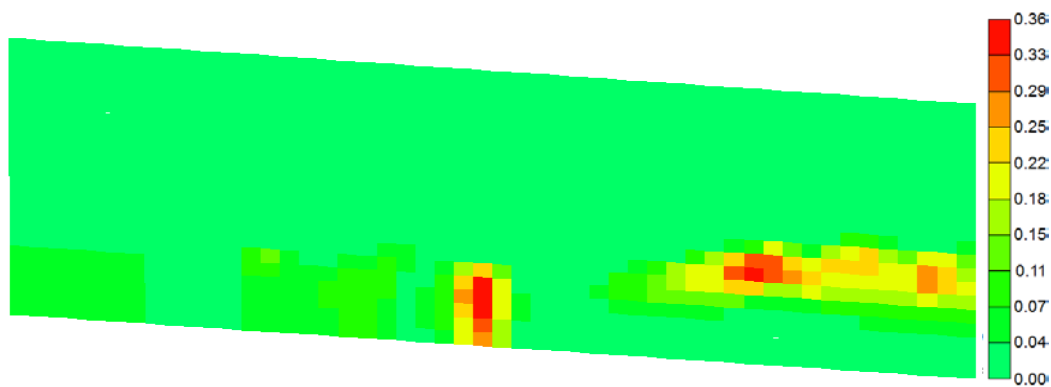


Figure 38: Gas saturation distribution in the domain.

Results and Discussion:

- The CO₂ hydrate saturation is non-uniform and generally high along the methane hydrate-water boundary separating Zone 1 and Zone 2. Free migration of the water phase is impeded between the zones and gas flow is increased from methane hydrate during the depressurization stage. The result suggests that the engaged scenario could be a promising approach for enhanced methane recovery with simultaneous CO₂ sequestration.
- The temperature of Zone 2 has increased significantly due to the formation of CO₂ hydrate combined with the pressure increase during CO₂ injection.
- The temperature and pressure conditions in all grid blocks were kept within the stability regions on the phase diagrams for CH₄ and CO₂ hydrates.

Task 3.0 Laboratory Hydrologic and Geomechanical Characterization and Analysis of Hydrate-Bearing Sediments

Subtask 3.1 Laboratory Measurement of Relative Permeability of CH₄ Gas in Brine-Saturated Hydrate-Bearing Sediments

- A literature review was conducted. Experimental studies on “gas-water” relative permeability measurements in hydrate-bearing sediments were found. The studies referred to the difficulties of inhibiting hydrate phase change (hydrate formation/dissociation) during gas flooding. They injected either cold CH₄ or N₂ gas

through water-saturated hydrate bearing samples within the CH₄ hydrate stability region but outside the N₂ hydrate stability region, to prevent hydrate dissociation or additional hydrate formation, respectively. However, they did not mention the possibility of additional CH₄ hydrate formation during the CH₄ injection within the CH₄ hydrate stability region, and that of CH₄ hydrate dissociation from the loss of CH₄ partial pressure during the N₂ injection.

- Procurement of test equipment and parts is in progress. Particularly, the ordering of the acoustic two-phase sonic fluid separator and back pressure regulators is complete. A design of new end plugs was proposed with larger fluid entrance, to prevent the fluid path from clogging by possible hydrate formation during the test.
- The retrofit of the environmental chamber continued. The installation of new gas lines and safety devices is complete. New electric lines and a temperature controller are being installed.
- A preliminary experimental procedure was developed. Main steps include:
 1. Water-saturated sand sample preparation (2-3 samples; F110 silica sand with D₅₀ = 120 μm).
 2. Base drainage relative permeability measurement by injecting CH₄ gas into water-saturated sand sample (S_h = 0%).
 3. Initial cementing hydrate formation at targeted S_h of about 20-50%.
 4. Non-cementing hydrate formation by brine injection slightly outside the brine (L_b)-H-V phase stability region and warming/cooling cycle.
 5. Drainage relative permeability measurement of brine-saturated hydrate-bearing sand sample (S_h = ~20-50%) by injecting CH₄ gas slightly outside the brine (L_b)-H-V phase stability region.

Subtask 3.2 Tri-Axial Compression Tests on Hydrate-Bearing Sediments with Induced Hydrate Dissociation under Shear Stress

- The modification of the test setup (including environmental chamber and mobile cart) was in progress.
- The small-strain mechanical property (acoustic property) of hydrate-bearing sediment during hydrate dissociation by depressurization was studied. The experimental data utilized in the study were obtained in FY14, after a geomechanical compression test on a non-cementing hydrate-bearing sample, as an extra data set. The sample, from which the data were obtained, therefore already had the loading history. **Error! Reference source not found.** shows the length and pore volume of the sample measured before the present study (in red).

Table 4: Changes in length and pore volume of hydrate-bearing sample, utilized in the present study, after the previous geomechanical compression test.

Unit of Measurement	Before Compression Test	After Compression Test and Reconsolidation
Length [mm]	99.6	86.8

Pore Vol. [ml]	75.5	81.7
Hydrate Vol. [ml]	36.7	36.7
S_h [%]	48.6	44.9

Despite the loading history on the sample, the present study could still reveal the influence of hydrate dissociation on the mechanical behaviors of hydrate-bearing sediments. The sequence of the hydrate dissociation of the sample was: (1) partial hydrate dissociation → (2) closing outlet valve → (3) P-T stabilization in closed-system → (4) repressurization into hydrate stability zone by injecting CH_4 -saturated CaCl_2 solution (hydrate reformation) → (5) repeat of the same cycle until the complete hydrate dissociation, as shown in **Error! Reference source not found.**

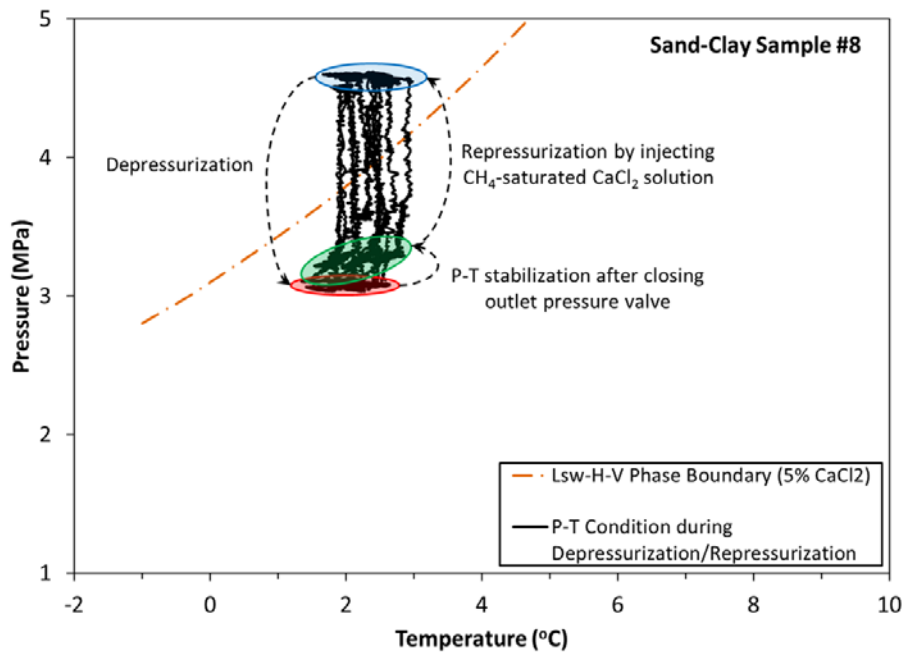


Figure 39: Path of P-T change during hydrate dissociation by depressurization, P-T stabilization in closed system, and hydrate reformation by repressurization.

The volume of dissociated CH_4 gas was measured during each depressurization process for hydrate saturation (S_h) calculations. Each acoustic wave measurement (**Error! Reference source not found.**) was then conducted after the residual gases were converted into hydrates by each repressurization process. As shown in **Error! Reference source not found.**, the arrival time of both P- and S-waves delayed as the hydrate dissociation progressed (S_h decreased). This indicates the progression of decrease in the stiffness of hydrate-bearing sediments during hydrate dissociation, and deduces the compressive deformation of hydrate reservoirs during gas production.

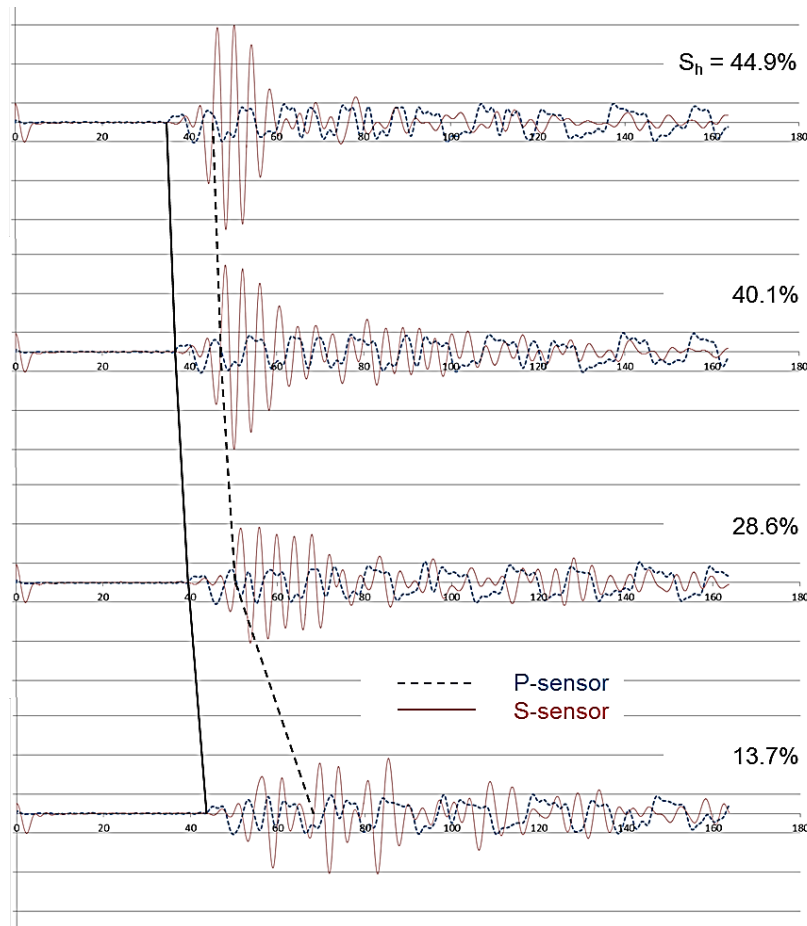


Figure 40: Progress of wave arrival delays after hydrate dissociations.

Subtask 3.3 Methodology Developments for Modeling Geomechanical Stability of Hydrate-Bearing Sediments under Hydrate Dissociation Condition

Effort has not begun on this subtask; pending supporting research staff emplacement.

Task 4.0 Pore-Scale Visualization and Characterization of Hydrate-Bearing Sediments

Subtask 4.1 Effect of Continuous Brine Flow on Hydrate Formation and Dissociation Behaviors

- The experimental setup including the cooling and illumination systems for the high-pressure microfluidic porous chip is complete (**Error! Reference source not found.**).

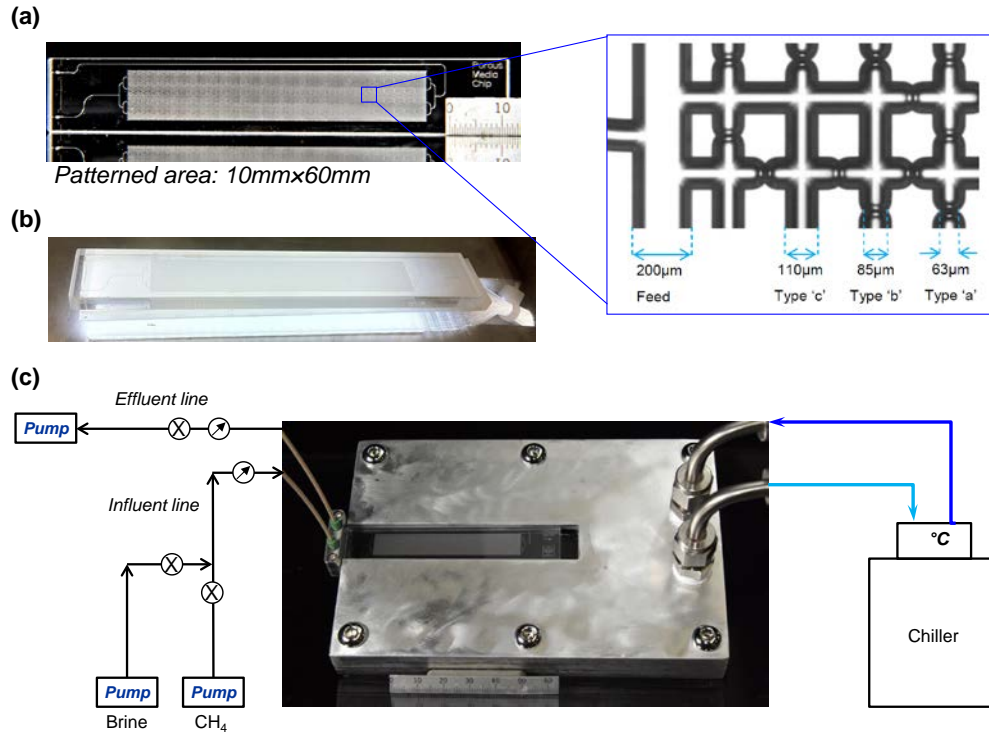


Figure 41: Microfluidic porous chip (a) porous space pattern, (b) illumination system, and (c) customized temperature control system.

Subtask 4.2 Water and Gas Distributions after Hydrate Dissociation and Implications to Permeability

- Pore network simulation (MATLAB codes) of gas or water percolation in hydrate-bearing sediments is complete (**Error! Reference source not found.**). The pore spaces were extracted from the CT images of natural sediments from the hydrate reservoir at the Mallik site.

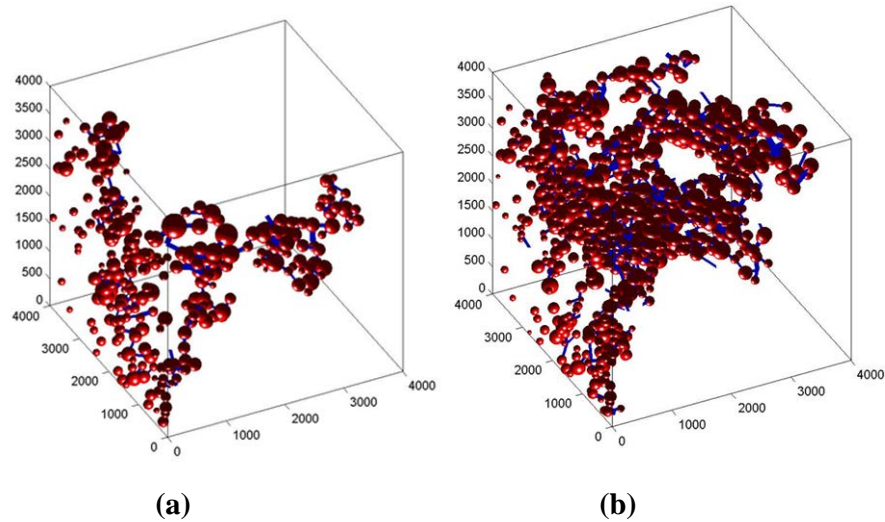


Figure 42: Pore network simulation based on 3D CT images - Percolation. (a) Left image: gas percolation through initially water-saturated hydrate-bearing sediments. (b) Right image: water percolation through initially gas-saturated hydrate-bearing sediments. The pore spaces are identical in both simulations and they are all extracted from the CT images of Mallik sand.

- Water retention curves in hydrate-bearing sediments were investigated and the van Genuchten model for hydrate-bearing sediments was modified.

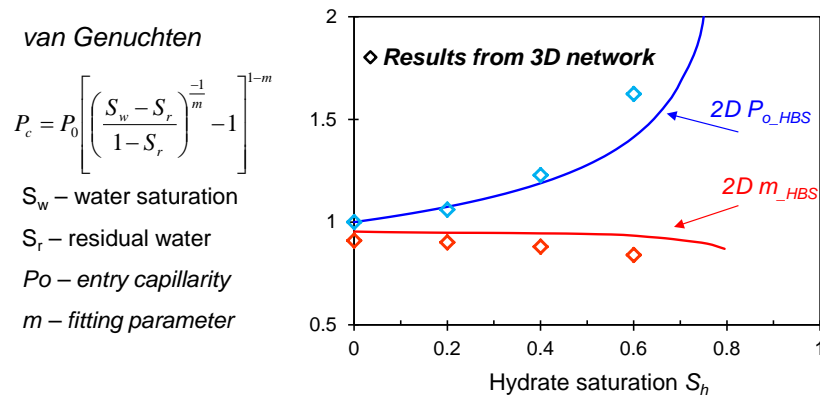


Figure 43: Modified van Genuchten model for hydrate-bearing sediments: both the P_0 and the m parameters in the van Genuchten model are hydrate saturation (S_h) dependent. Solid lines are results from 2D pore network simulation results and diamonds are 3D results (blue for P_0 and red for m).

Subtask 4.3 Links between Hydrate Morphologies and Geomechanical Properties

- Installing piezocrystals for both P-/S-waves measurements in hydrate-bearing sediments in in progress.

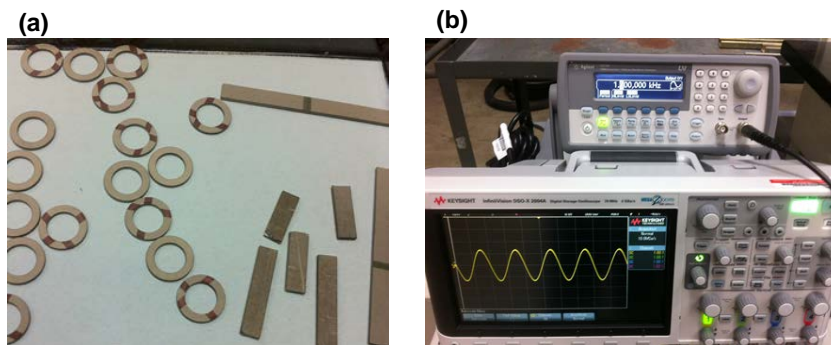


Figure 44: Wave characterization of hydrate-bearing sediments. (a) Annular p-wave piezocrystals and bender element for s-wave measurement. (b) A function generator is triggering a 1 kHz sinusoidal wave signal that is captured by the oscilloscope.

Subtask 4.4 Microfluidic-Based Permeability of Hydrate-Bearing Sediments

- The Cooling System, Imaging System, and Thermal Transfer Plate construction are complete and functionally tested. The system is currently functional, with minor modifications performed as needed during various tests. Redundant Temperature Controllers are on-hand in case of failure.
- Construction of the THF/Water flow system is complete and has been tested. The system is typically used at atmospheric pressure, but pressurization is possible.
- A new lens was specified and purchased for the Zeiss Stemi 2000-C Microscope to allow imaging of the entire height of the Microfluidic Chip. Images captured during the THF/Water flow testing using the existing low-resolution camera prove that the new lens does image the entire height of the chip.

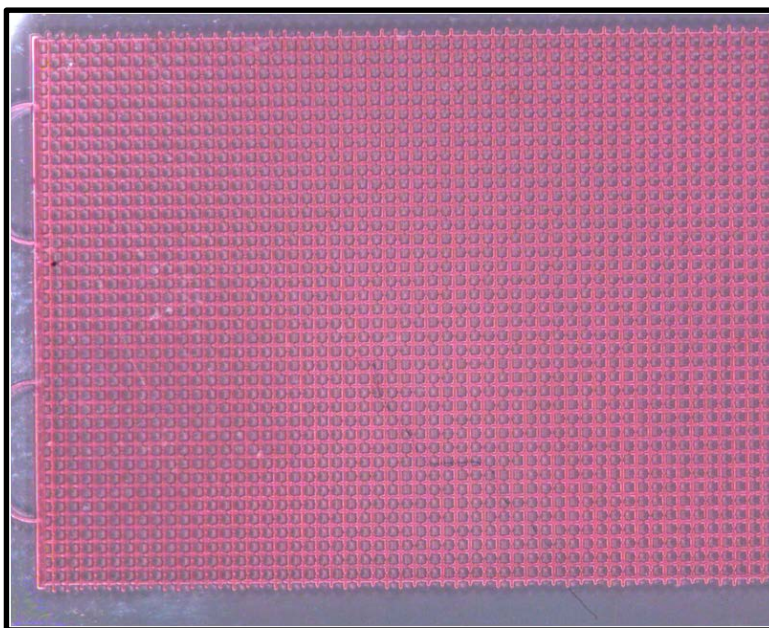


Figure 45: THF/Water with red dye - total height of microfluidic chip is shown in the image. This image was made using the lowest zoom setting on the Zeiss Stemi 2000-C microscope.

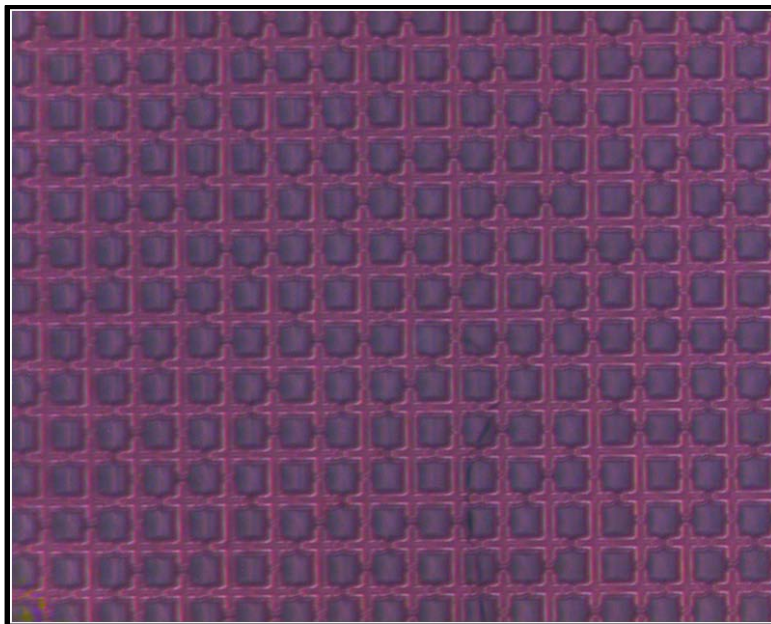


Figure 46: THF/water with red dye - image of microfluidic chip using highest zoom setting on the Zeiss Stemi 2000-C microscope. Individual cells are readily visible in the image.

- Modifications to the Microfluidic Chip were made to provide:
 - A hold-down mechanism for the microfluidic chip. The hold-down mechanism consists of magnets attached to the copper plate which interact with identical magnets on an aluminum hold-down bar.
 - A non-interfering background for imaging. The non-interfering background is white paint on the copper plate. Use of foil tape and the plain copper bar yielded poor images due to reflections and lighting issues.

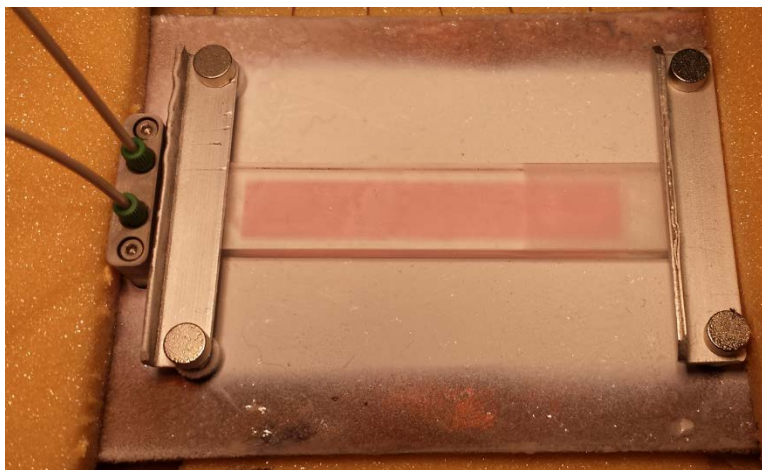


Figure 47: THF/water flow test in the microfluidic chip. Note the magnetic hold-down assembly and the white background on the copper bar.

- Additional parts were specified and ordered for the imaging and cooling system.
 - A new high-resolution camera was ordered to allow detailed imaging of the microfluidic chip. The current camera has low resolution. The new camera is expected to arrive in May 2015.
 - A second circulating chiller was ordered to provide separate cooling for the relays. Currently, the Peltier Plates and relays are cooled using the same chiller. During extended runs, the amount of heat produced by the system may overrun the cooling capacity of one chiller. A second chiller will be used to separate the Peltier Plates from the relays to reduce the risk of overheating.
 - A spare microfluidic chip was ordered and received. This spare chip will be available to NETL users in case of failure or other issues.
- An attempt to make THF Hydrate was made in the Microfluidic Chip in March 2015. A mixture of 40% THF/60% H₂O (by weight) mixed with red food dye was introduced into the chip and cooling was applied. The mixture reached a temperature of less than 1°C for over 24 hours. No hydrate was detected.
- After failing to make THF Hydrate in the Microfluidic Chip, a separate test was conducted in a laboratory refrigerator using dyed THF/Water mixtures placed in a bottle. It was discovered that red food dye does not form transparent THF Hydrate (if any hydrate is formed, at all). A red solid is formed using the red dye, but it may be ice and not hydrate. When the experiment was attempted with blue food dye, a transparent solid was formed and a blue liquid remained in the bottle. Future experiments will use only blue food dye.



Figure 48: THF/water mixtures placed in laboratory refrigerator. The bottle on the left has solid crystals that have little or no blue dye in them. The bottle on the right has all crystals with red dye in them. The red dye will not be used in experimentation.

Forecast for Next 6 Months

Task 1.0 Project Management and Outreach

The FY15-Q2 Report will be submitted on April 30, 2015.

Task 2.0 Reservoir Simulation of Gas Hydrates Production Field Tests

Subtask 2.1 Alaska North Slope Production Test Simulation Assistance

- The next level of complexity will incorporate a heterogeneous distribution of hydrate saturation which can be obtained from a porosity-hydrate saturation correlation inferred from L106 well logs. Reservoir simulations are in progress for a single realization of porosity distribution with uniform hydrate saturation of 0.5.
- Flow simulations will be conducted for multiple realizations subsequently to predict gas and water production rates and determine the critical design and operational factors that would affect production and thoroughly describe uncertainties in the model predictions.
- Within the next four months, a representative 3D heterogeneous model of the L-pad C and D-sands, with respect to porosity, hydrate saturation, and other intrinsic reservoir properties, will be developed.
- Production test design schemes will be recommended based on the model predictions.

Subtask 2.2 International Code Comparison Continuation – Ignik Sikumi History Match Analysis and Marine Deposit Based on the 2013 Nankai Trough Test or Other Marine Sites

- An equilibrated domain will be considered before injecting CO_{2(g)} into the reservoir domain. The long term focus is on creating a 3D heterogeneous domain and studying the effect of CO₂ hydrate formation on methane production.

Task 3.0 Laboratory Hydrologic and Geomechanical Characterization and Analysis of Hydrate-Bearing Sediments

Subtask 3.1 Laboratory Measurement of Relative Permeability of CH₄ Gas in Brine-Saturated Hydrate-Bearing Sediments

- The literature review will continue. (FY15-Q3)
- Preliminary experimental methodology for the relative measurements will be developed, reviewed, and completed. (FY15-Q3)
- The temperature chamber will be ready for the test by adding new gas lines, a temperature controller, and gas detectors. (FY15-Q3)
- New equipment and parts will be assembled into the mobile cart. (FY15-Q3)
- The experimental method and test setup will be examined by conducting preliminary tests. (FY15-Q3)
- The first planned test will be conducted, and its result will be analyzed. (FY15-Q4)

Subtask 3.2 Tri-Axial Compression Tests on Hydrate-Bearing Sediments with Induced Hydrate Dissociation under Shear Stress

- An overall test plan will be completed. (FY15-Q3)
- Modification of the existing geomechanical test setup will be completed in accordance with the test plan. (FY-Q3)

- An initial compression test will be conducted, simultaneously examining the test plan and setups. (FY15-Q3)
- Planned tests will be completed and results will be analyzed and reported. (FY15-Q4)

Subtask 3.3 Methodology Developments for Modeling Geomechanical Stability of Hydrate-Bearing Sediments under Hydrate Dissociation Condition

Effort has not begun on this subtask; pending identification of research staff on the task. The team hopes to validate the constitutive model with experimental data on the modeling of dissociation on stress-strain behavior. The team would also conduct and develop benchmark tests for validating the coupling analysis for geomechanics analysis of operational scenarios, for use in such cases as methane extraction from the ground.

Task 4.0 Pore-Scale Visualization and Characterization of Hydrate-Bearing Sediments

Subtask 4.1 Effect of Continuous Brine Flow on Hydrate Formation and Dissociation Behaviors

- To follow the NETL's recipe of forming noncementing hydrate and obtain CT images of hydrate pore habits at each critical step using the Be vessel.

Subtask 4.2 Water and Gas Distributions after Hydrate Dissociation and Implications to Permeability

- To obtain CT images of residual water and gas distributions after hydrate distribution.
- To simulate the gas percolation process during hydrate dissociation.

Subtask 4.3 Links between Hydrate Morphologies and Geomechanical Properties

- To use the Be-vessel with new endcaps to study effects of hydrate morphologies on the measured p-wave velocity and strength of hydrate-bearing sediments.
- To use Al-vessel to study the hydrate distribution on measurement p- and s-wave characteristics.

Subtask 4.4 Microfluidic-Based Permeability of Hydrate-Bearing Sediments

Continuing during FY15-Q3, experiments with THF hydrate will be conducted to further test the Microfluidic Chip system and determine the ability to process images from the experiments. Initial images will be obtained using the existing low-resolution camera. Additional images will be analyzed using a higher resolution camera that will be delivered and installed during FY15-Q3. Image processing will be conducted with ImageJ to determine the saturation of THF hydrate in the Microfluidic Chip.

The goal of the experimentation will be to correlate hydrate density to flow, which will show how the permeability of the microfluidic chip changes as hydrate density increases. Once initial testing of THF hydrates is complete, a temperature gradient will be induced to increase the density of hydrate formed, attempting to mimic real world hydrate densities.

During FY15-Q4, making CO₂ Hydrate will be attempted using the Microfluidic Chip system. The system as constructed can operate under pressure, so a system redesign to handle CO₂ should not be needed.

Products

Publications, Conference Papers, and Presentations

Seol, Y., Choi, J.H., Dai, S., Jarvis, K., “Recent Advances in NETL's Laboratory Studies of Hydrate-Bearing Sediments,” *Fire in the Ice*, 15 (1), 5-9, 2015.

Changes/Problems

There is a potential delay in deploying the Be-vessel for hydrate studies, as few other projects behind schedules are engaging the Be vessel and the micro-XCT. Aluminum core holders are being designed to be used for Industrial CT (Subtask 4.1 and Subtask 4.3).

Fiscal Year 2015 Quarter 3

Accomplishments

Task 1.0 Project Management and Outreach

The FY15-Q3 deliverables included:

- The FY15-Q2 Report was submitted to SCNGO on April 30, 2015.

Task 2.0 Reservoir Simulation of Gas Hydrates Production Field Tests

Subtask 2.1 Alaska North Slope Production Test Simulation Assistance

- An anisotropic 3D heterogeneous reservoir model based on the PBU L-pad hydrate accumulation in ANS was created (Figure 49). The model including Unit D, C1, and C2 hydrate-bearing sand employs geostatistical realizations of the porosity field honoring porosity values derived from 78 well logs in the L-Pad area. The porosity-dependent hydrate saturation distribution and horizontal/vertical permeability are also applied to the model.
- Four well designs were used to estimate gas production potential over 30 years of hydrate depressurization at 2.7 MPa of the bottom hole pressure (Figure 50). The draft of the paper devoted to gas production from the reservoir model utilizing various scenarios and well designs is being prepared.

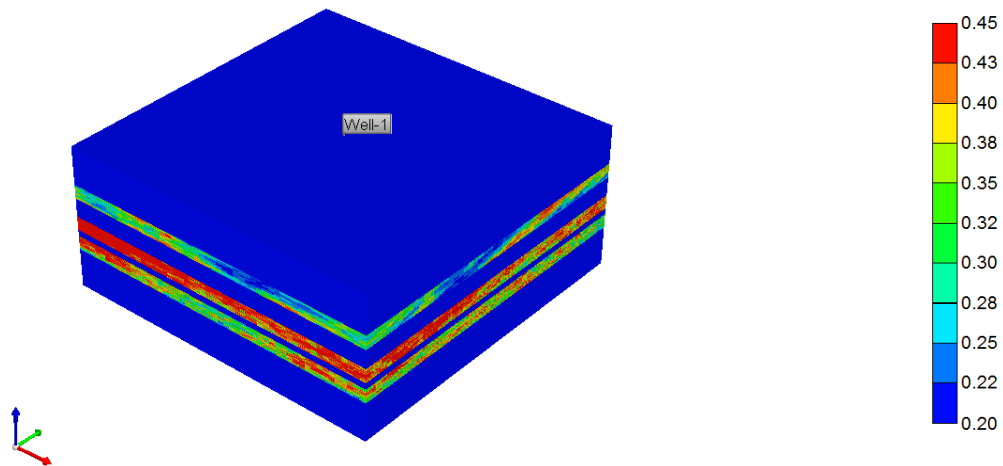


Figure 49: The 3D reservoir model of the D and C sands showing porosity distribution. The layers in blue represent shale.

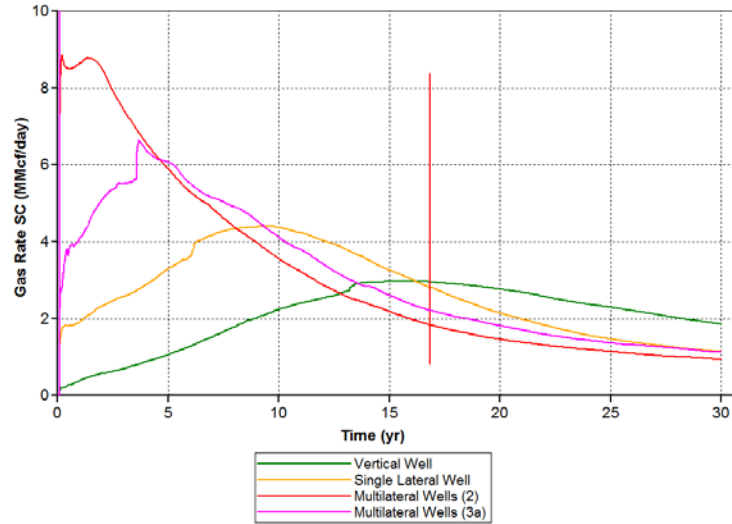


Figure 50: Gas production rates from the reservoir model using various well designs.

Subtask 2.2 International Code Comparison Continuation – Iñik Sikumi History Match Analysis and Marine Deposit Based on the 2013 Nankai Trough Test or Other Marine Sites

Accomplishments:

- A Class 2 inclined hydrate reservoir model was developed based on the P/T conditions that existed at the Iñik Simuki site (Figure 51). Simulation of CO₂ injection into water-saturated zone was completed to convert the free water into immobile hydrate phase.

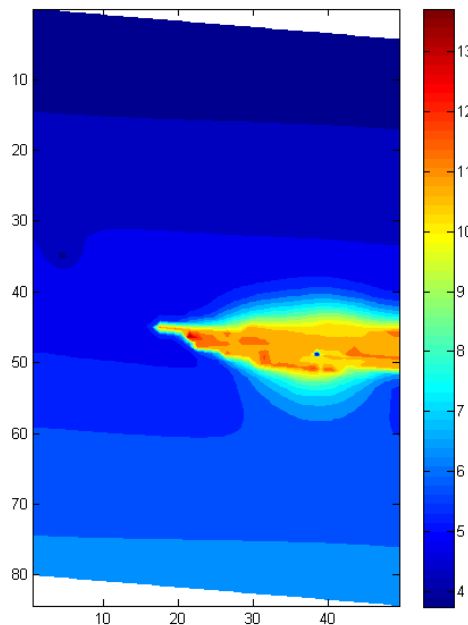


Figure 51: Temperature profile (°C) of the reservoir showing temperature increase due to CO₂ hydrate formation underneath the methane hydrate zone after 75 days of CO₂ injection.

Task 3.0 Laboratory Hydrologic and Geomechanical Characterization and Analysis of Hydrate-Bearing Sediments

Subtask 3.1 Laboratory Measurement of Relative Permeability of CH₄ Gas in Brine-Saturated Hydrate-Bearing Sediments

- Procurement of test equipment and parts is in progress. Fabrication of new end plugs with a larger fluid entrance, which was designed to prevent the clogging of fluid path by possible hydrate formation during the test, was completed. The leak-check test was also conducted on the new plugs.
- Fabrication of acoustic two-phase sonic fluid separator and back pressure regulators by a private company are underway and they will be delivered in mid-August.
- The retrofit of the environmental chamber was completed along with its test run.

Subtask 3.2 Tri-Axial Compression Tests on Hydrate-Bearing Sediments with Induced Hydrate Dissociation under Shear Stress

- The modification of test setup was completed with the addition of a mass flow meter and a balance.
- The first tri-axial test on the HBS sample under hydrate dissociation condition was conducted. The mixture of sand-5% clay was utilized to form the host sample, and the non-cementing hydrate was formed in the host sample by utilizing the brine-injection method. Throughout the entire course of hydrate formation, the effective confining pressure (σ'_o) of 0.69 MPa was maintained. The porosity of ~0.36 and hydrate saturation (S_h) of ~45% were attained in the sample. Below are the experimental steps applied to the tri-axial test:

Step (1): Under constant effective confining pressure (σ'_o) of 0.69 MPa and drainage condition, the deviator stress, q (effective axial pressure, σ'_a – effective confining pressure, σ'_o) was raised to ~4 MPa, the stress level which is higher than the strength of the host sample and lower than that of the HBS sample (with $S_h = \sim 45\%$). This stress condition refers to as “metastable”.

Step (2): The deviator stress (i.e., axial, confining, and pore pressures) was maintained constant, until the volume change of the sample ceased or slowed down.

Step (3): Upon observing little change in sample volume, the pore pressure was lowered from ~5.5 MPa to ~3 MPa, to dissociate the hydrate.

Step (4): After the dissociation was finished, the pore pressure was raised back to ~5.5 MPa.

Step (5): Once the displacement of axial piston approached its maximum limit, the axial pressure was lowered below ~6.2 MPa from ~9.5 MPa.

- The data analysis of the first test was conducted. Figure 52 shows the histories of stress, axial strain, and volumetric strain over the time of the tri-axial test. Especially, to present the stress history during the test, the stress ratio of deviator stress (q) to mean effective pressure (p') was utilized instead of showing all the pressure parameters, where the mean effective pressure, $p' = (\sigma'_a + 2\sigma'_o)/3$. From the results, the following observations were made:

Step (1): During the q application, normal axial and volumetric behaviors of the sample were observed, i.e., the sample axially contracts, while its volume initially contracts and then starts to expand (dilatancy).

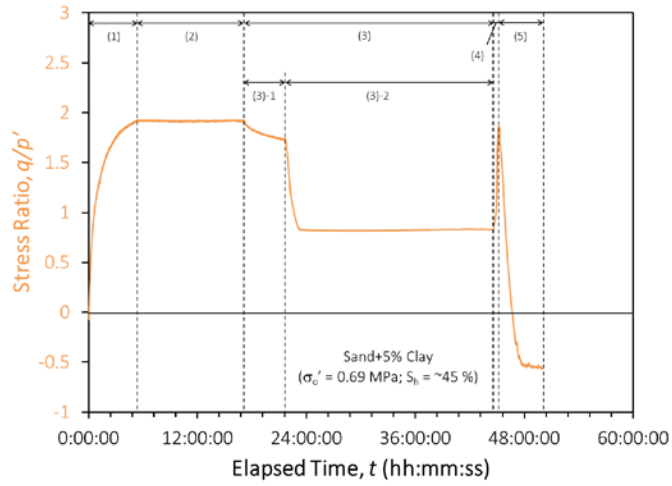
Step (2): At constant q at ~ 4 MPa, the sample continued to axially contract, while the volume of sample increased (dilatancy). At the q applied, the axial and volumetric changes may continue until a certain large strain is reached.

Step (3): While the pore pressure was lowered to dissociate the hydrate, the axial contraction and volume expansion were slowed down, due to the increased effective confining pressure. The change of the volume even turned into the contractive direction. In this step, the increased effective pressure could be a more dominant factor on the behavior of the sample than the loss of hydrate by the dissociation.

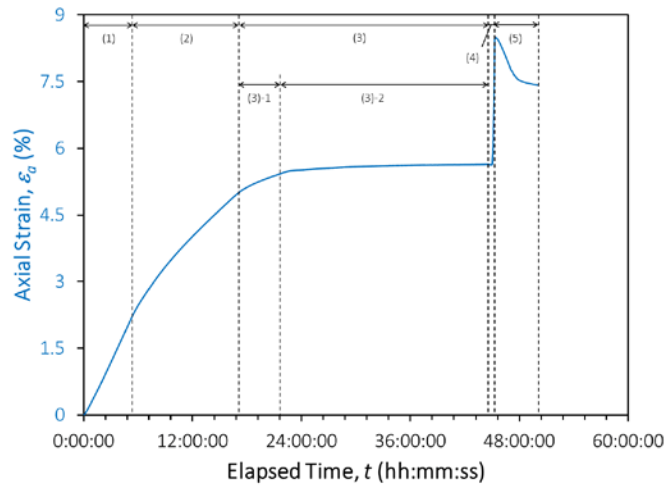
Step (4): During the pore pressure raise, drastic increases in axial contraction and volumetric expansion were observed. The loss in load-bearing capacity of hydrates between soil particles after the hydrate dissociation, along with the decrease in the effective confining pressure, caused the abrupt failure behavior.

Step (5): The axial pressure was lowered when the maximum-allowed axial displacement of the system was reached. The release in axial pressure, while maintaining the same effective confining pressure, allowed the sample to axially extend and volumetrically contract.

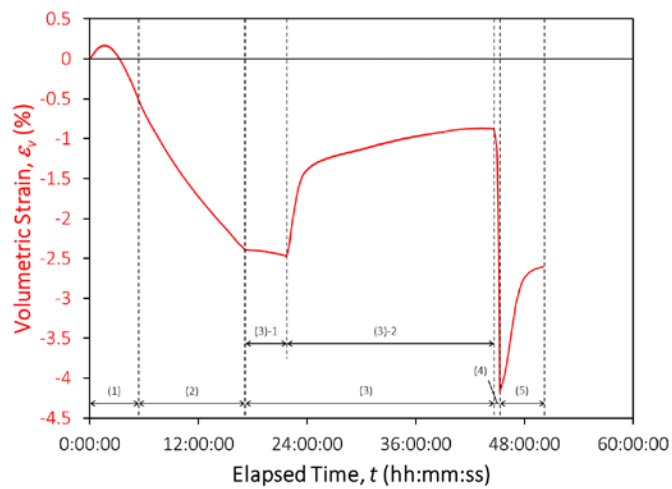
- The experimental results imply that the HBS reservoir dissociated by depressurization can collapse when the pore pressure is recovered from the surroundings.



(a)



(b)



(c)

Figure 52: Histories of stress, axial strain, and volumetric strain over the time of tri-axial test on HBS sample under dissociation by depressurization. (a) stress ratio of deviator stress to mean effective pressure, q/p' , where $q = \sigma_a' - \sigma_v'$ and $p' = (\sigma_a' + 2\sigma_v')/3$, (b) axial strain, ϵ_a , and (c) volumetric strain, ϵ_v .

Further description of Figure 52 is as follows: Step (1): application of $q = \sim 4$ MPa, Step (2): maintaining q at ~ 4 MPa, Step (3): lowering pore pressure from ~ 5.5 MPa to ~ 3 MPa for dissociation, Step (4): raising pore pressure back to ~ 5.5 MPa, and Step (5): lowering axial pressure. [Note: At Step (3)-1, the pore pressure valve from the sample was closed, to redirect the drainage line to the mass flow meter prior to hydrate dissociation, which caused the drop of pore pressure in association with the ongoing straining from Step (2). After the redirection of drainage line, the pore pressure valve was reopened before lowering the pore pressure for dissociation (Step (3)-2). Positive strains represent the contraction.]

Subtask 3.3 Methodology Developments for Modeling Geomechanical Stability of Hydrate-Bearing Sediments under Hydrate Dissociation Condition

This task began June 1, 2015. Implementation of the constitutive model into FLAC3D has begun with the start of this task, while the coupling of FLAC3D with Tough+Hydrate continues.

The stability of sediments that contain methane hydrate under dissociation has been studied using two triaxial test environments: stress-controlled and strain-controlled. (1) Stress-controlled triaxial tests in FLAC3D have been developed to test a framework for modeling laboratory test results. The soils are modeled after those obtained by Miyazaki et al. and Lin et al., 2015.

(2) During a strain control test, a representative sample $S_H=40\%$ under a confining pressure of 3MPa reached a peak strength of about 10MPa, and with further straining passing the peak strength, the soil is softened to a shear stress of about 8.2MPa at a vertical strain of 25%. A hydrate free soil, namely with $S_H=0\%$, under the same confining pressure, reached a peak strength of 7.5 MPa, and then softened to about 6.2 MPa at 25% (Figure 53).

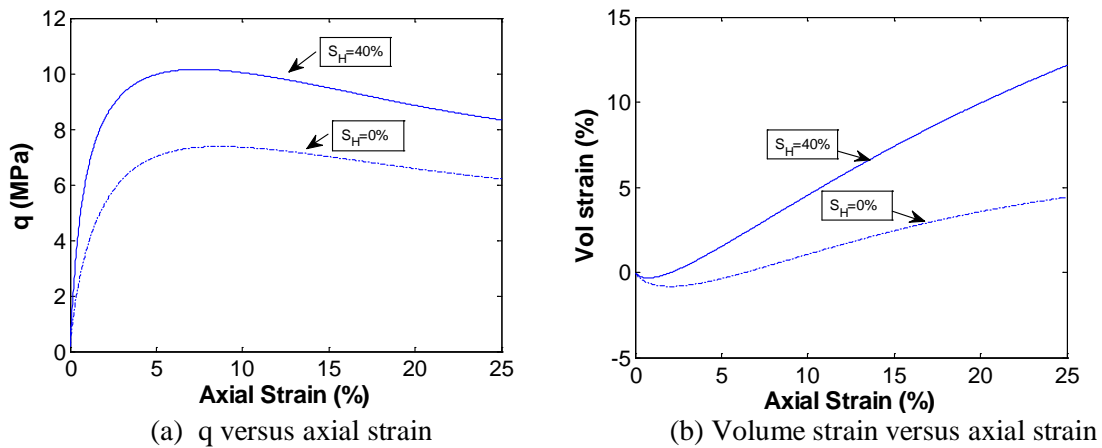
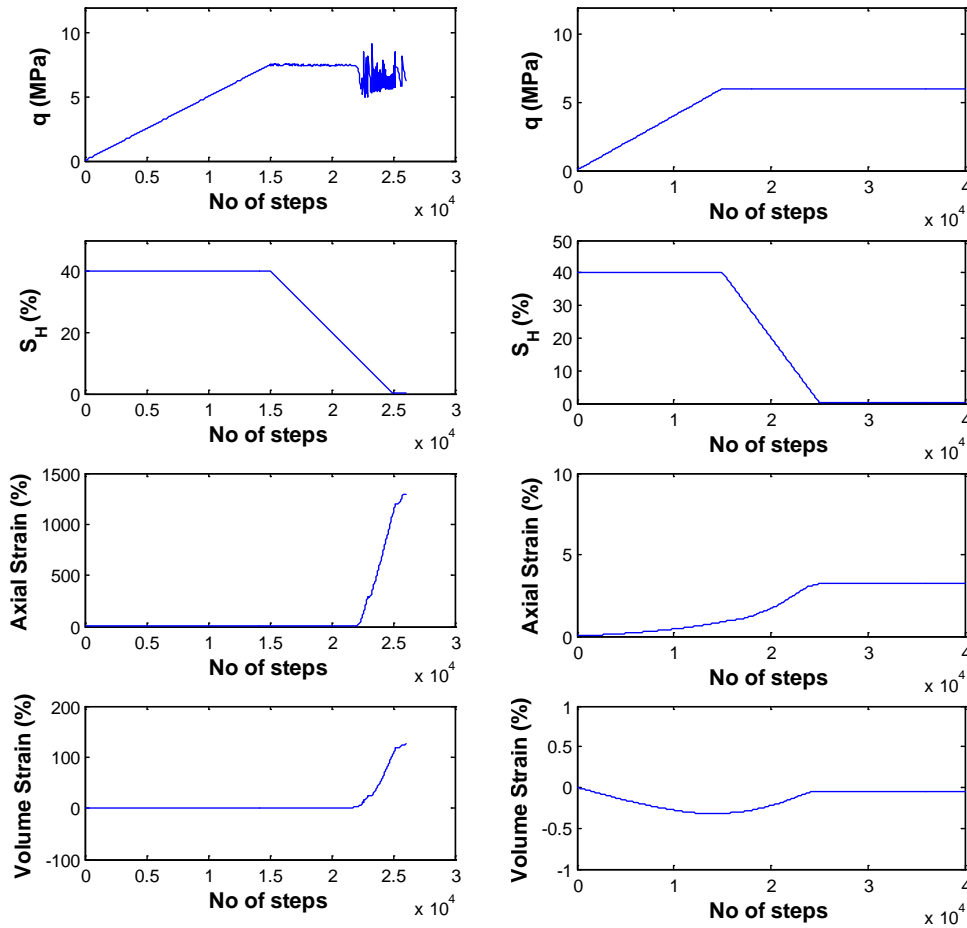


Figure 53: The stress-strain behavior of a soil under strain controlled test with hydrate saturation unchanged.

With this background, it is expected that if a soil’s shear to strength is greater than 7.5 MPa, upon dissociation it would become unstable. For affirming this in the model, a stress controlled test was first conducted on a hydrate bearing sample with $S_H=40\%$, and shear it to a shear stress, q , of 8 MPa, and then initiate dissociation over 20,000 steps to reach complete dissociation. The results

indeed showed that even before the hydrate was completely dissociated, the axial strain would accelerate so fast and the sample simply became unstable with both the axial strain and the volume strain. Then the test was repeated allowing only the q to reach 6 MPa upon initiating dissociation. For the latter case, the sample remained stable (Figure 54).

The results obtained demonstrate that the research should be carried out further with more careful tuning on parameter inputs.



(a) Shear to $q=7.5$ MPa then dissociate (b) Shear to $q=6$ MPa then dissociate

Figure 54: Stress controlled test with hydrate dissociation after the shear stress, q , reach a certain value.

References:

Lin, J.S., Seol, Y., and Choi, J., “An SMP Subloading Critical State Model for Methane Hydrate-Bearing Soils”, *International Journal for Numerical and Analytical Methods in Geomechanics*, 2015; 39:969-987.

Miyazaki, K., Masui, A., Sakamoto, Y., Aoki, K., Tenma, N., Yamaguchi, T., 2011. “Triaxial Compressive Properties of Artificial Methane-Hydrate-Bearing Sediment,” *J. Geophys. Res.*, 116, B06102.

Task 4.0 Pore-Scale Visualization and Characterization of Hydrate-Bearing Sediments

Subtask 4.1 Effect of Continuous Brine Flow on Hydrate Formation and Dissociation Behaviors

- Preliminary test: water injection. The illumination gives sufficient contrast for imaging the two-phase flow (i.e., air and water). This provides the base for further investigation of relative permeability measurement in hydrate bearing sediments using this set up.
- Preliminary test: nucleation of ice. The cooling system can sufficiently lower the temperature below the freezing point and cause ice nucleation within the microfluidic chip. The nucleation of methane hydrate within the microfluidic chip is ongoing (Figure 55).

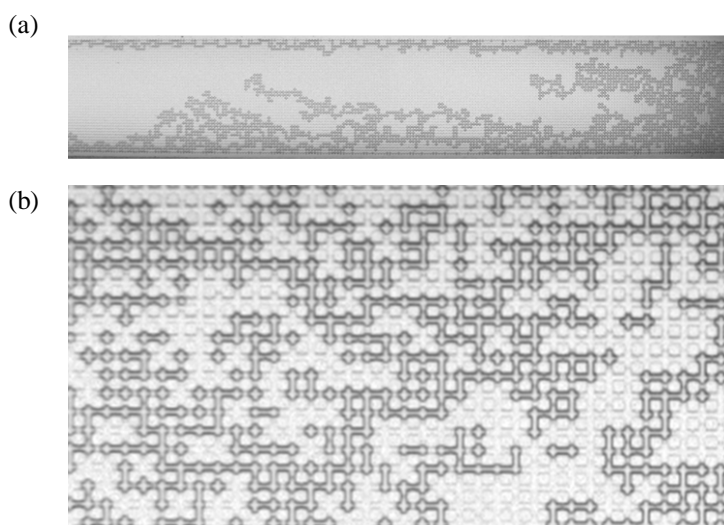


Figure 55: Microfluidic porous chip. (a) Water injection into dried microfluidic chip: image across the whole chip. (b) Ice nucleation in patches within the partially water saturated chip. White grids: ice saturated tubes; black grids: air saturated tubes.

Subtask 4.2 Water and Gas Distributions after Hydrate Dissociation and Implications to Permeability

- Pore network simulations: effects of hydrate distribution (distributed vs. patchy) on relative permeability. The pore networks are extracted from 3D CT images of sands from the Mallik hydrate site (Figure 56).

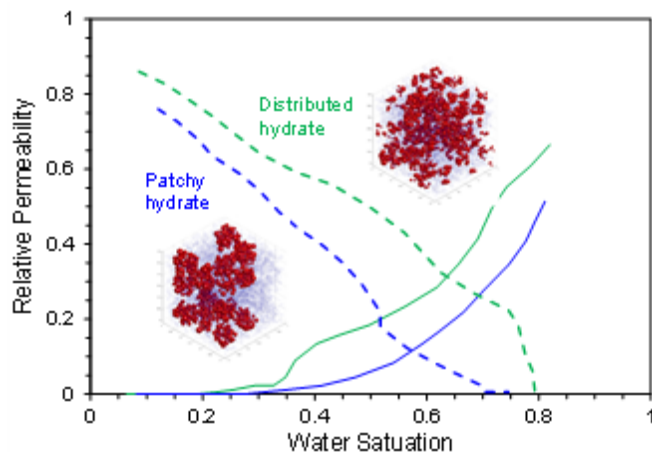


Figure 56: CT imaging based pore network simulation: effects of hydrate distribution on relative permeability.

- In general, sediments with distributed hydrates tend to result in higher both gas and water permeability during hydrate dissociation than that in sediments with patchy hydrates (Figure 57). This mainly because the gas and water phases from hydrate dissociation can more readily form percolation paths in sediments with distributed hydrates than that with patchy hydrates (Note: simulations from the ASU group show similar results).

Subtask 4.3 Links between Hydrate Morphologies and Geomechanical Properties

- Preliminary test: ice nucleation in sands and measured wave velocities.

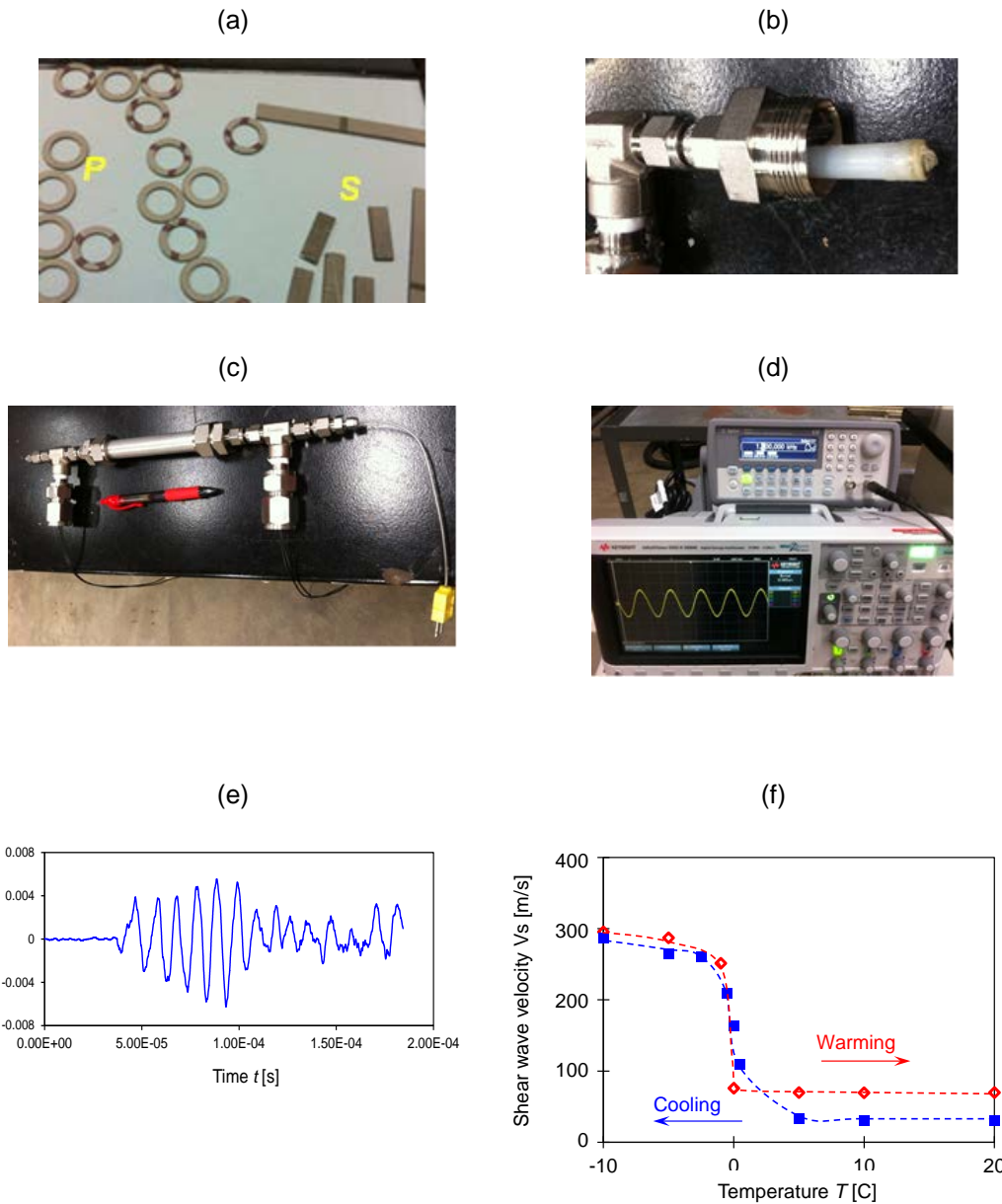


Figure 57: The Al-vessel to study the linkage between hydrate morphology and measured wave characteristics. (a) Bender elements for S-wave measurement and circular rings for P-wave measurement. (b) Instrumented Teflon probe with P-/S-wave piezocrystals. (c) Overview of the Al-vessel instrumented with a pair of P-wave and S-wave piezocrystals and a K-type thermocouple. (d) Electronics (i.e., a signal generator and an oscilloscope) for wave measurements. (e) Obtained S-wave signature. (f) Evolution of S-wave velocity during the freezing (blue data) and thawing (red data) of partially water saturated sands (initial water saturation is 30%).

Subtask 4.4 Microfluidic-Based Permeability of Hydrate-Bearing Sediments

- A thorough literature search found that Methyl-Blue dye has been used in previous hydrate experiments to aid in visualization. Methyl-Blue is too large to be included in hydrate formation but also is excluded during ice formation. This requires more precise control of the temperature during hydration formation studies to prevent the sample from freezing instead of forming hydrate.



Figure 58: Water with .01% weight of methyl blue dye frozen in freezer.



Figure 59: Close up of the same solution as previous figure.

- Construction of a dehumidifying chamber was completed and placed into service, which allows for sub cooling of the microchip without the buildup of moisture and ice impairing visualization.

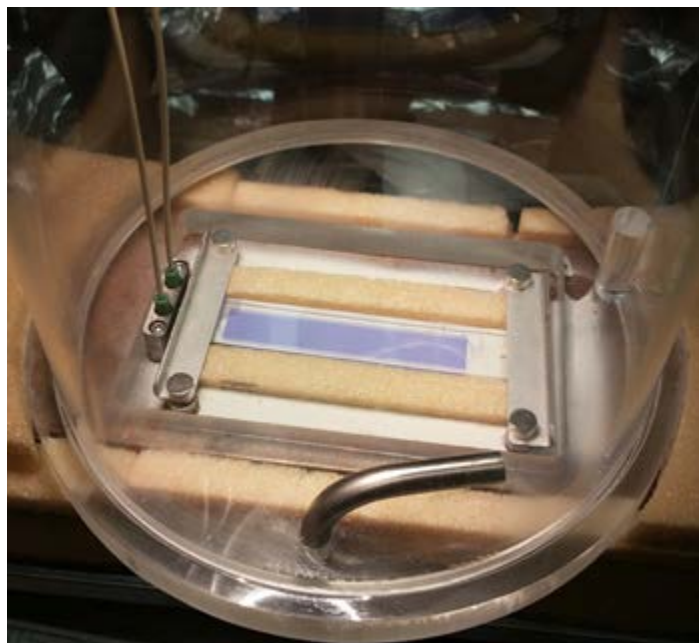


Figure 60: Humidity chamber with "house" supplied dry air continuously flowing.

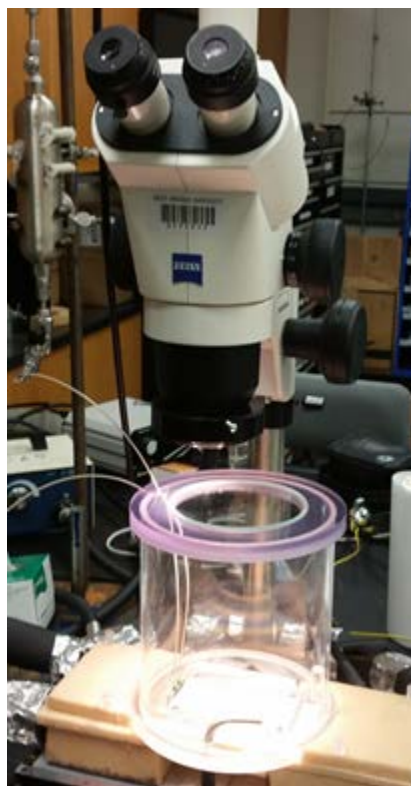


Figure 61: Humidity chamber installed over the chip and under the microscope.

- A previously ordered, spare microfluidic chip has arrived and will be held as backup for the current chip.
- A previously ordered cooling bath arrived in May but has not been released for use at my offsite facility. No expected date has been given for when this will be released.
- A previously ordered high definition camera arrived in May but has not been released for use at my offsite facility. No expected date has been given for when this will be resolved.
- Ten percent (10%) weight solution of THF/water was used to find the optimal conditions for hydrate formation. Using the max cooling capabilities of the PET plates, a temperature gradient was created along the length of the chip. This consisted of approximately -10°C to -4°C which produced a visual change in the chip.

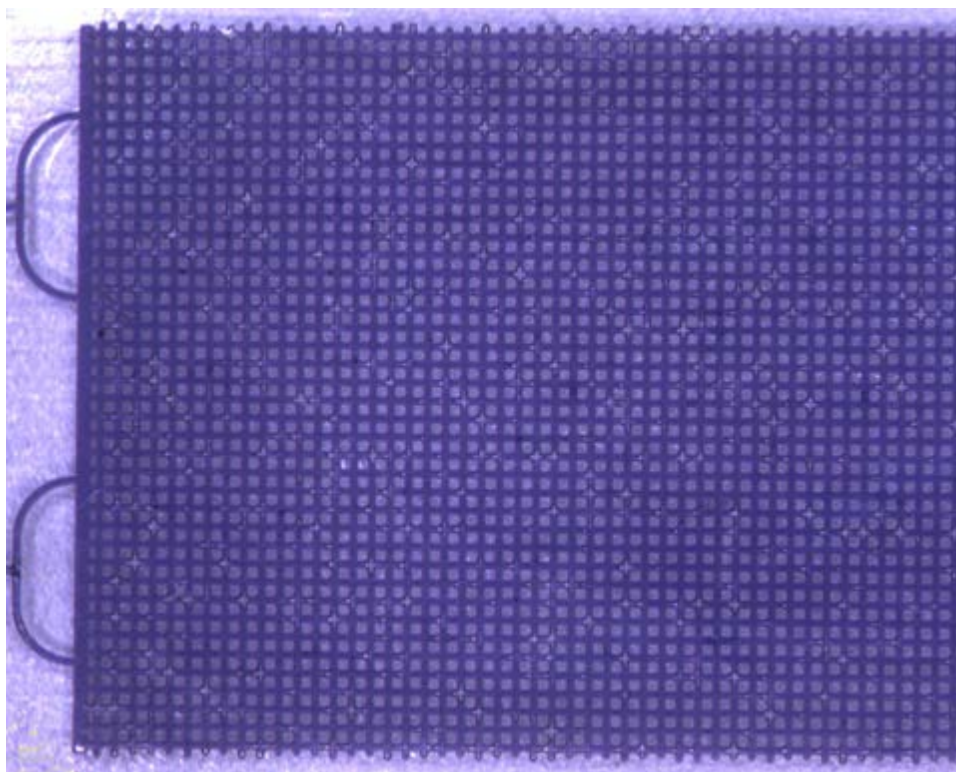


Figure 62: Image captured during initial hydrate formation experiments. The lighter blue areas in the pore spaces formed during sub cooling and are thought to be ice.

It was believed that this was documentation of hydrate formation. However, due to the extreme sub cooling it could possibly be ice instead of hydrate (Figure 62). However, the cooling bath could not maintain the level of cooling and overheated, causing the researcher (Mr. Terry Ryan) to abort this attempt. This result has yet to be repeated. Different THF/Water solution concentrations are being explored to reproduce this result and then verify the formation of hydrate.

Forecast for Next 6 Months

Task 1.0 Project Management and Outreach

The FY15-Q3 Report will be submitted on July 30, 2015.

Task 2.0 Reservoir Simulation of Gas Hydrates Production Field Tests

Subtask 2.1 Alaska North Slope Production Test Simulation Assistance

- The sensitivity analysis will be continued for (1) comparison with previous results of gas production from the simplistic reservoir models, (2) secondary hydrate evaluation from the perspective of anisotropic heterogeneity of porosity and hydrate saturation, and (3) economic assessment to support recommendations for well design, and currently is expected to be finished by September 30, 2015. The paper on gas production from the reservoir model utilizing various scenarios and well designs is expected to be prepared for submission into a peer-reviewed international journal by Sept 30, 2015 as well.

Subtask 2.2 International Code Comparison Continuation – Iñnik Sikumi History Match Analysis and Marine Deposit Based on the 2013 Nankai Trough Test or Other Marine Sites

- The simulations of gas production from the homogeneous and heterogeneous Class 2 incline reservoir models will be conducted at two initial conditions. First, hydrate depressurization will be invoked with mobile water zone at the base of hydrate stability; and second, the depressurization will be induced after the water-saturated zone is converted into immobile CO₂ hydrate-bearing zone.

Task 3.0 Laboratory Hydrologic and Geomechanical Characterization and Analysis of Hydrate-Bearing Sediments

Subtask 3.1 Laboratory Measurement of Relative Permeability of CH₄ Gas in Brine-Saturated Hydrate-Bearing Sediments

- Development of preliminary experimental methodology for the relative measurements will be reviewed and completed. (FY15-Q4)
- New equipment and parts will be assembled into the mobile cart. (FY15-Q4)
- The experimental method and test setup will be examined by conducting preliminary tests. (FY15-Q4)
- The planned tests will be conducted, and their result will be analyzed. (FY15-Q4 and FY16-Q1)

Subtask 3.2 Tri-Axial Compression Tests on Hydrate-Bearing Sediments with Induced Hydrate Dissociation under Shear Stress

- Two or three more planned tests will be conducted at the different initial deviator stresses and dissociation methods, and their results will be analyzed and reported. (FY15-Q4 and FY16-Q1)

Subtask 3.3 Methodology Developments for Modeling Geomechanical Stability of Hydrate-Bearing Sediments under Hydrate Dissociation Condition

- FLAC3D and TOUGH+Hydrate will be coupled in modeling the dissociation behavior.
- Various scenarios of dissociation will be tested beyond laboratory test setup.
- The soil behavior will be modeled after reconsolidation.

Task 4.0 Pore-Scale Visualization and Characterization of Hydrate-Bearing Sediments

Subtask 4.1 Effect of Continuous Brine Flow on Hydrate Formation and Dissociation Behaviors

- The formation of methane hydrate within the microfluidic chip is ongoing. The next step is to inject brine at particular pressure-temperature conditions (between the stability bounds for hydrate in fresh water and brine systems) and observe hydrate pore habit change. Consequent hydrate dissociation also provides results for Subtask 4.2.

Subtask 4.2 Water and Gas Distributions after Hydrate Dissociation and Implications to Permeability

- The sands (at 10MPa confining stress) from Mallik hydrate site were scanned; the pore network from micro-CT images of this sample were extracted; the pore network simulation based on this network was performed with artificially generated hydrates; the effects of hydrate saturation on the parameters of the van Genuchten model were investigated; and the effects of hydrate distribution on relative gas and water permeability during hydrate distribution were studied. Hence, the major goals of this subtask have been accomplished at this stage.
- A complementary study will be done to conduct CT scanning of THF hydrate bearing sediments. Hydrate morphology that formed dissolved phase within the sediments will be studied in collaboration with the Arizona State University group to investigate water retention curves and relative permeability simulations based on the CT scanning results.

Subtask 4.3 Links between Hydrate Morphologies and Geomechanical Properties

- Synthesis of methane hydrate in sands using the Al-vessel and measurements on the sample stiffness (i.e., wave velocities) will be performed along with CT scanning for the hydrate morphology.

Subtask 4.4 Microfluidic-Based Permeability of Hydrate-Bearing Sediments

Continuing during FY15-Q4, experiments with THF hydrate will be conducted to further test the Microfluidic Chip system and determine the ability to process images from the experiments. Initial images will be obtained using the existing low-resolution camera. A higher resolution camera will be delivered and installed during FY15-Q4. Additional images will be analyzed using the high-resolution camera. Image processing will be conducted with ImageJ to determine the saturation of THF hydrate in the Microfluidic Chip.

The goal of the experimentation will be to correlate hydrate density to flow, which will show how the permeability of the microfluidic chip changes as hydrate density increases. Once initial testing of THF hydrates is complete, a temperature gradient will be induced to increase the density of hydrate formed, attempting to mimic real world hydrate densities.

During FY16-Q1, making CO₂ Hydrate using the Microfluidic Chip system will be attempted. The system, as constructed, can operate under pressure, so a system redesign to handle CO₂ should not be needed.

Products

Publications, Conference Papers, and Presentations

Dai, S., Cha, J., Seol, Y., Rosenbaum, E., and Zhang, W., “Thermal Conductivity Measurements in Unsaturated Hydrate-Bearing Sediments,” submitted for *Geophysical Research Letters* on May 12, 2015.

Mahabadi, N., Zheng, X., Dai, S., Seol, Y., Zapata, C.E., and Jang, J., “Soil Water Characteristic Curves in THF Hydrate-Bearing Sediments, Experimental Measurement and Pore-network Model Simulation,” abstract submitted for Geo-Chicago 2016 on May 5, 2015.

A session for the AGU fall meeting has been organized:

- B040: Hydrate bearing sediments: characterization, modeling, and implications on geohazard and gas production.
- Conveners are: Jeen-Shang Lin (Pitt), Yongkoo Seol (NETL), Timothy J Kneafsey (LBNL), and Marcelo J Sanchez (TAMU).

Changes/Problems

There is a potential delay on Task 4.0 as the current researcher, Dr. Sheng Dai will leave for a new faculty position. It is expected for him to continue the work until September 30, 2015.

Appendix A: Participating and Other Collaborating Organizations

Table A-1 includes the name and organization of all federal, URS/AECOM, university, and ORISE participants. Each quarter, changes or additions will be shown in **highlighted yellow text**.

**Table A-1: Natural Gas Hydrates Research Portfolio
 Participating and Collaborating Organizations**

Task/Subtask Number – Name	Name	Organization
Task 1.0 Project Management and Outreach		
Subtasks 1.1-1.4 Project Management and Outreach	Gary Sames Yongkoo Seol	NETL-ORD
	Jeffery Ilconich	URS/AECOM
Subtask 1.5 Outreach	Yongkoo Seol	NETL-ORD
	Jeffery Ilconich	URS/AECOM
Subtask 1.6 Portfolio Management	Yongkoo Seol	NETL-ORD
	Jeffery Ilconich	URS/AECOM
Task 2.0 Reservoir Simulation of Gas Hydrates Production Field Tests		
Subtask 2.1 Alaska North Slope Production Test Simulation Assistance	Yongkoo Seol	NETL-ORD
	Taiwo Ajayi Prathyusha Sridhara	ORISE
Subtask 2.2 International Code Comparison Continuation – Igñik Sikumi History Match Analysis and Marine Deposit Based on the 2013 Nankai Trough Test or Other Marine Sites	Yongkoo Seol	NETL-ORD
	Taiwo Ajayi Prathyusha Sridhara	ORISE
Task 3.0 Laboratory Hydrologic and Geomechanical Characterization and Analysis of Hydrate-Bearing Sediments		
Subtask 3.1 Laboratory Measurement of Relative Permeability of CH ₄ Gas in Brine-Saturated Hydrate-Bearing Sediments	Yongkoo Seol	NETL-ORD
	Jeong-Hoon Choi	ORISE
Subtask 3.2 Tri-Axial Compression Tests on Hydrate-Bearing Sediments with Induced Hydrate Dissociation under Shear Stress	Yongkoo Seol	NETL-ORD
	Jeong-Hoon Choi	ORISE
Subtask 3.3 Methodology Developments for Modeling Geomechanical Stability of Hydrate-Bearing Sediments under Hydrate Dissociation Condition	Yongkoo Seol	NETL-ORD
	TBD	TBD

Task/Subtask Number – Name	Name	Organization
Task 4.0 Pore-Scale Visualization and Characterization of Hydrate-Bearing Sediments		
Subtask 4.1 Effect of Continuous Brine Flow on Hydrate Formation and Dissociation Behaviors	Yongkoo Seol	NETL-ORD
	Sheng Dai Terrance Ryan Matthew Tacker	ORISE
Subtask 4.2 Water and Gas Distributions after Hydrate Dissociation and Implications to Permeability	Yongkoo Seol	NETL-ORD
	Sheng Dai Terrance Ryan Matthew Tacker	ORISE
Subtask 4.3 Links between Hydrate Morphologies and Geomechanical Properties	Yongkoo Seol	NETL-ORD
	Sheng Dai Terrance Ryan Matthew Tacker	ORISE
Subtask 4.4 Microfluidic-Based Permeability of Hydrate-Bearing Sediments	Yongkoo Seol	NETL-ORD
	Sheng Dai Terrance Ryan Matthew Tacker	ORISE